Journal of Computational Physics **168,** 286–315 (2001)
doi:10.1006/jcph.2001.6691, available online at http://www.idealibrary.com on IDEAL®

A Staggered Fourth-Order Accurate Explicit Finite Difference Scheme for the Time-Domain Maxwell's Equations[1]

Amir Yefet and Peter G. Petropoulos

Department of Mathematical Sciences, New Jersey Institute of Technology, University Heights, Newark, New Jersey 07102
E-mail: yefet@m.njit.edu, peterp@m.njit.edu

Received November 16, 1999; revised December 18, 2000

We consider a model explicit fourth-order staggered finite-difference method for the hyperbolic Maxwell's equations. Appropriate fourth-order accurate extrapolation and one-sided difference operators are derived in order to complete the scheme near metal boundaries and dielectric interfaces. An eigenvalue analysis of the overall scheme provides a necessary, but not sufficient, stability condition and indicates long-time stability. Numerical results verify both the stability analysis, and the scheme's fourth-order convergence rate over complex domains that include dielectric interfaces and perfectly conducting surfaces. For a fixed error level, we find the fourth-order scheme is computationally cheaper in comparison to the Yee scheme by more than an order of magnitude. Some open problems encountered in the application of such high-order schemes are also discussed.

Key Words: Maxwell's equations, staggered finite-difference schemes, fourth-order schemes, FD-TD scheme.

1. INTRODUCTION

Many modern technology applications involve the propagation and scattering of transient electromagnetic signals, e.g., electronic on-chip interconnects, nondestructive testing of concrete structures, and aircraft radar signature analysis. The design and optimization of new systems demands fast and accurate solvers of the time-domain Maxwell equations over complex closed/open domains filled with heterogeneous dielectrics in which metals

[1] Supported by AFOSR Grant F49620-99-1-0072 and AFOSR MURI Grant F49620-96-1-0039.

0021-9991/01 $35.00

are embedded. This is a challenge for numerical modelers as the relevant mathematical problem to be solved generally exhibits disparate spatial (e.g., inhomogeneities with both small- and large-scale features) and time (e.g., dispersive media) scales. A mini-review of the computational electromagnetics (CEM) state of the art can be found in [1].

Thus far, Yee's [2–3] finite-difference time-domain (FD-TD) algorithm has provided the best [4] second-order accurate nondissipative direct solution of the time-domain Maxwell equations on a staggered grid. The numerical error is controlled solely by the mesh size, and the scheme is particularly easy to implement in the presence of heterogeneous dielectrics and perfectly conducting (PEC) boundaries; it is second-order convergent for planar geometries, where boundaries/interfaces occur on grid points. As all finite difference schemes, the Yee scheme is dispersive and anisotropic, and for large-scale problems, or for problems requiring long-time integration of Maxwell's equations, errors from dispersion and anisotropy quickly accumulate and become significant unless a fine discretization is used [6]. This leads to prohibitive memory requirements and high computational cost when addressing real-world problems.

For some time now, workers in CEM have realized the promise of high-order finite-difference schemes [5–12]. The question of staggered versus unstaggered high-order schemes has been studied in [13] which showed that, for a given order of accuracy, a staggered scheme is more accurate and efficient than an unstaggered scheme. However, the extended spatial stencil of staggered high-order methods has inhibited their wide acceptance as it does not allow the easy application of boundary conditions (far-field, impedance, or metal) and the accurate modeling of dielectric interfaces. In this paper we revisit the explicit(2, 4) scheme of [5], and we use it as a model to address some of the remaining objections to using high-order stencils on a staggered grid. Although it is possible to consider a fourth-order time integrator with Fang's spatial differencing, e.g. [18], we concentrate on the particular (2, 4) scheme herein in order to introduce and study appropriate spatial differencing techniques for bounded domains.

We adopt a domain-decomposition point of view and treat dielectric interfaces as boundary points between subdomains in which the spatial derivatives are computed to fourth-order accuracy; boundary data is imposed as in the Yee scheme. For the model fourth-order spatial stencil, we propose a series of numerical boundary conditions, involving one-sided differentiation and extrapolation/interpolation, to implement metal boundaries and dielectric interfaces when these occur on electric field grid points. Where appropriate, we indicate how to modify our scheme for the cases where the boundaries, or the dielectric interfaces, occur on magnetic field grid points. Our approach is motivated by [15, 16], which considered the accurate treatment of dielectric interfaces for the second-order Yee scheme (a similar approach for second-order schemes is developed in [17]). The treatment of metal boundaries herein is different from that used in [6], where the method of images was applicable because of the infinite extent of those boundaries in the numerical tests performed there. Also, the treatment of dielectric interfaces herein is different from that in [7], where a simple pointwise specification of dielectric properties was used; we show that such an approach severely degrades the convergence rate of the scheme. A stability analysis, which includes the effects of metal boundaries and dielectric interfaces, is given. We find the necessary CFL stability condition derived in [5] also holds when metal boundaries are present, while problems with dielectric interfaces require a slightly smaller CFL number which we determine for a given mesh size and dielectric contrast. For the model scheme herein this is not overly restrictive as one typically chooses a CFL number proportional to the mesh size

in order to compute fourth-order accurate results. Numerical experiments show that these new numerical boundary conditions preserve the fourth-order accuracy of the scheme when boundaries/interfaces occur on grid points. We also examine the effect of stair-stepping a boundary not aligned with the grid, and of the presence of geometric singularities.

2. PRELIMINARIES

The Maxwell equations in an isotropic, homogeneous, nondispersive medium are

$$\begin{aligned} \frac{\partial \mathbf{B}}{\partial t} + \nabla \times \mathbf{E} &= 0 \quad \text{(Faraday's Law)}, \\ \frac{\partial \mathbf{D}}{\partial t} - \nabla \times \mathbf{H} &= 0 \quad \text{(Ampere's Law)}, \\ \mathbf{B} &= \mu \mathbf{H}, \\ \mathbf{D} &= \epsilon \mathbf{E}. \end{aligned} \tag{1}$$

In the absence of impressed electric charge, the magnetic induction and electric displacement fields satisfy the constraints (Gauss's law):

$$\begin{aligned} \nabla \cdot \mathbf{B} &= 0, \\ \nabla \cdot \mathbf{D} &= 0. \end{aligned} \tag{2}$$

Scattering obstacles will be modeled by a spatial variation of ϵ and μ. In free space, ϵ and μ are constant, equal to their minimum values ϵ_0, μ_0. The speed of light in free space is $c = \frac{1}{\sqrt{\epsilon_0 \mu_0}}$.

To simplify the notation we will mainly consider two-dimensional problems. In two dimensions, (1) decouples into two independent sets of equations, each representing a distinct polarization. We shall use as our model system of equations those of the transverse magnetic (TM) polarization, where the electric field is a scalar while the magnetic field is a plane vector,

$$\begin{aligned} \frac{\partial E_z}{\partial t} &= \frac{1}{\epsilon}\left(\frac{\partial H_y}{\partial x} - \frac{\partial H_x}{\partial y}\right), \\ \frac{\partial H_x}{\partial t} &= -\frac{1}{\mu}\frac{\partial E_z}{\partial y}, \\ \frac{\partial H_y}{\partial t} &= \frac{1}{\mu}\frac{\partial E_z}{\partial x}. \end{aligned} \tag{3}$$

Because the fields have no $\hat{z}$-dependence, Gauss' Law is trivially satisfied by $\mathbf{D} = (0, 0, \epsilon E_z)^T$, while the magnetic fields are constrained to satisfy $\nabla \cdot (\mu H_x, \mu H_y, 0)^T = 0$ for all time. Wave excitation is achieved by imposing appropriate initial and/or boundary conditions. We will present numerical examples for dielectrics with (a) piecewise-constant ϵ ($\mu = \mu_0$), and (b) piecewise-constant μ ($\epsilon = \epsilon_0$). Case (b) can be thought (duality) to represent the transverse electric (TE) polarization problem for a dielectric of piecewise-constant ϵ and fixed $\mu = \mu_0$. The extension of the work herein to the more general three-dimensional problem (1) is straightforward.

3. THE SCHEME IN A HOMOGENEOUS BOUNDED DIELECTRIC

The discretization of (3) with the staggered Yee scheme ($O(\Delta t^2)$-accurate leapfrog time integration) is

$$\begin{aligned} E_{z,i,j}^{n+1} &= E_{z,i,j}^{n} + \frac{\Delta t}{\epsilon \Delta x}\delta_x H_{y,i,j}^{n+1/2} - \frac{\Delta t}{\epsilon \Delta y}\delta_y H_{x,i,j}^{n+1/2}, \\ H_{x,i,j-1/2}^{n+1/2} &= H_{x,i,j-1/2}^{n-1/2} - \frac{\Delta t}{\mu \Delta y}\delta_y E_{z,i,j-1/2}^{n}, \\ H_{y,i-1/2,j}^{n+1/2} &= H_{y,i-1/2,j}^{n-1/2} + \frac{\Delta t}{\mu \Delta x}\delta_x E_{z,i-1/2,j}^{n}, \end{aligned} \tag{4}$$

where

$$\begin{aligned} \delta_x U_{i,j} &= U_{i+1/2,j} - U_{i-1/2,j}, \\ \delta_y U_{i,j} &= U_{i,j+1/2} - U_{i,j+1/2}. \end{aligned} \tag{5}$$

Hereafter we shall refer to (4) and (5) as the Yee scheme.

In the fourth-order scheme [5] the spatial difference operators (5) are replaced by fourth-order accurate stencils. For example, to compute a fourth-order accurate approximation of the quantity $\Delta y \frac{\partial U}{\partial y}|_{(i,j+1/2)}$ we use

$$\delta_y U_{i,j} = \frac{1}{24}(U_{i,j-1} - 27U_{i,j} + 27U_{i,j+1} - U_{i,j+2}). \tag{6}$$

The Yee scheme can be applied at all nodes in a bounded domain except at the first and last where boundary conditions are to be imposed. However, the fourth-order stencil requires numerical boundary conditions at the nodes next to an electric field boundary node. To complete this scheme at the two interior grid points (one electric and one magnetic) immediately next to the first and last electric field grid points of a bounded domain, we use fourth- and third-order accurate one-sided approximations in order to globally approximate the derivative. No physical boundary conditions are included at this stage. These one-sided approximations are

$$\begin{aligned} \frac{\partial U}{\partial y_{i,1/2}} &= \frac{1}{24\Delta y}(-22U_{i,0} + 17U_{i,1} + 9U_{i,2} - 5U_{i,3} + U_{i,4}), \\ \frac{\partial U}{\partial y_{i,1}} &= \frac{1}{24\Delta y}\left(-23U_{i,1/2} + 21U_{i,3/2} + 3U_{i,5/2} - U_{i,7/2}\right), \\ \frac{\partial U}{\partial y_{i,N-1}} &= \frac{1}{24\Delta y}\left(23U_{i,N-1/2} - 21U_{i,N-3/2} - 3U_{i,N-5/2} + U_{i,N-7/2}\right), \\ \frac{\partial U}{\partial y_{i,N-1/2}} &= \frac{1}{24\Delta y}(22U_{i,N} - 17U_{i,N-1} - 9U_{i,N-2} + 5U_{i,N-3} - U_{i,N-4}), \end{aligned} \tag{7}$$

for the derivative in the $\hat{y}$-direction with truncation errors $\frac{71\Delta y^4}{1920}\frac{\partial^5 U}{\partial y^5}$ and $\frac{\Delta y^3}{24}\frac{\partial^4 U}{\partial y^4}$, and similarly for the derivative in the $\hat{x}$-direction. Consequently, electric field boundary conditions can be imposed as in the Yee scheme. Labeling the scheme, which employs (6) in the interior and (7) near the boundary, a $4-3-4-3-4$ scheme (see [14] for similar notation), we have also tested alternative boundary treatments that result in $4-4-4-4-4$,

$3-4-4-4-3$, or $3-3-4-3-3$ schemes; such schemes were rejected through numerical experimentation as less accurate.

We next define

$$\mathbf{A_H} = \begin{bmatrix} -23 & 21 & 3 & -1 & . & . & 0 \\ 1 & -27 & 27 & -1 & . & . & 0 \\ 0 & 1 & -27 & 27 & -1 & . & 0 \\ . & . & . & . & . & . & \\ 0 & . & . & 1 & -27 & 27 & -1 \\ 0 & . & . & 1 & -3 & -21 & 23 \end{bmatrix}, \tag{8}$$

and

$$\mathbf{A_E} = \begin{bmatrix} -22 & 17 & 9 & -5 & 1 & . & 0 \\ 1 & -27 & 27 & -1 & . & . & 0 \\ 0 & 1 & -27 & 27 & -1 & . & 0 \\ . & . & . & . & . & . & \\ 0 & . & . & 1 & -27 & 27 & -1 \\ 0 & . & -1 & 5 & -9 & -17 & 22 \end{bmatrix}, \tag{9}$$

so the matrix form of the approximation to the $\hat{y}$-derivative at the midpoint between grid points, and at the grid points, is respectively

$$\frac{\partial}{\partial y}\begin{bmatrix} U_{i,1/2} \\ U_{i,3/2} \\ . \\ . \\ U_{i,N-1/2} \end{bmatrix} = \frac{1}{24\Delta y}\mathbf{A_E}\begin{bmatrix} U_{i,0} \\ U_{i,1} \\ . \\ U_{i,N-1} \\ U_{i,N} \end{bmatrix},$$

$$\frac{\partial}{\partial y}\begin{bmatrix} U_{i,1} \\ U_{i,2} \\ . \\ . \\ U_{i,N-1} \end{bmatrix} = \frac{1}{24\Delta y}\mathbf{A_H}\begin{bmatrix} U_{i,1/2} \\ U_{i,3/2} \\ . \\ U_{i,N-3/2} \\ U_{i,N-1/2} \end{bmatrix},$$

and similarly for the derivative in the $\hat{x}$-direction. With these definitions, the matrix form of the discrete TM equations (3) is

$$\begin{aligned} [EZ_{i,j}]^{n+1} &= [EZ_{i,j}]^n + \frac{\Delta t}{24\epsilon\Delta x}\mathbf{A_H}\left[HY_{i+1/2,j}\right]^{n+1/2} - \frac{\Delta t}{24\epsilon\Delta y}\left[HX_{i,j+1/2}\right]^{n+1/2}\mathbf{A_H^t}, \\ \left[HX_{i,j+1/2}\right]^{n+1/2} &= \left[HX_{i,j+1/2}\right]^{n-1/2} - \frac{\Delta t}{24\mu\Delta y}[EZ_{i,j}]^n\mathbf{A_E^t}, \\ \left[HY_{i+1/2,j}\right]^{n+1/2} &= \left[HY_{i+1/2,j}\right]^{n-1/2} + \frac{\Delta t}{24\mu\Delta x}\mathbf{A_E}[EZ_{i,j}]^n. \end{aligned} \tag{10}$$

Hereafter we shall refer to (10) as the explicit(2,4) scheme.

We now demonstrate that (10) is divergence-free for TM waves, i.e., that

$$\frac{\partial}{\partial t}\nabla\cdot(\mu H_x, \mu H_y)^T = 0. \tag{11}$$

From the second and third equations in (10) it is easy to see that the following holds

$$\left(\frac{1}{24\Delta x}\mathbf{A_E}\left[(\mu HX)_{i,j+1/2}\right]+\frac{1}{24\Delta y}\left[(\mu HY)_{i+1/2,j}\right]\mathbf{A_E^t}\right)^{n+1/2}$$
$$-\left(\frac{1}{24\Delta x}\mathbf{A_E}\left[(\mu HX)_{i,j+1/2}\right]+\frac{1}{24\Delta y}\left[(\mu HY)_{i+1/2,j}\right]\mathbf{A_E^t}\right)^{n-1/2}=0. \qquad (12)$$

This is the discrete form of (11) at spatial location $(i+1/2,\ j+1/2)$ (the center of the rectangular cell with corners at the nearest-neighbor electric nodes) and time level n on the grid since

$$\frac{1}{24\Delta x}\mathbf{A_E}\left[(\mu HX)_{i,j+1/2}\right]=\left[\frac{\partial(\mu HX)}{\partial x}\right]_{i+1/2,j+1/2}+O(\Delta x^4)$$
$$\frac{1}{24\Delta y}\left[(\mu HY)_{i+1/2,j}\right]\mathbf{A_E^t}=\left[\frac{\partial(\mu HY)}{\partial y}\right]_{i+1/2,j+1/2}+O(\Delta y^4).$$

Hence, if the field is numerically divergence-free initially, i.e., the initial data satisfies (2), it will remain so ever after. We have determined that (12) holds in numerical simulations to within $O(10^{-13})$. If the permeability μ is discontinuous, the derivation of the divergence-free property differs. In that case we segment the domain into subdomains, and then (11) holds in each region.

If the perfect conductor is located on a tangential magnetic field node, then a different treatment is required as now a homogeneous Neumann condition, $\frac{\partial H_{tang}}{\partial n}=0$, holds on such a node. We shall explain the necessary modifications using the one-dimensional case involving HY and EZ; the extension to two and three dimensions follows along similar lines. On the perfect conductor, $\frac{\partial HY}{\partial x}^{n+1/2}_{i=1/2}=0$ is the boundary condition to be imposed. Now, the electric field node at $i=1$ is viewed as a boundary node for which we must obtain an update that takes into account the boundary condition at $i=1/2$. To that effect we obtain the required $\frac{\partial HY}{\partial x}^{n+1/2}_{i=1}$ by a fourth-order interpolation of the fluxes at neighboring electric field nodes and at the boundary node

$$\frac{\partial HY}{\partial x}^{n+1/2}_{i=1}=\frac{16}{35}\frac{\partial HY}{\partial x}^{n+1/2}_{i=1/2}+\frac{\partial HY}{\partial x}^{n+1/2}_{i=2}-\frac{3}{5}\frac{\partial HY}{\partial x}^{n+1/2}_{i=3}+\frac{1}{7}\frac{\partial HY}{\partial x}^{n+1/2}_{i=4}.$$

Using the physical boundary condition at $i=1/2$ (where the flux is known) this reduces to

$$\frac{\partial HY}{\partial x}^{n+1/2}_{i=1}=\frac{\partial HY}{\partial x}^{n+1/2}_{i=2}-\frac{3}{5}\frac{\partial HY}{\partial x}^{n+1/2}_{i=3}+\frac{1}{7}\frac{\partial HY}{\partial x}^{n+1/2}_{i=4}. \qquad (13)$$

We approximate $\frac{\partial HY}{\partial x}^{n+1/2}_{i=3,4}$ by using (6), and $\frac{\partial HY}{\partial x}^{n+1/2}_{i=2}$ by using the second formula in (7), so the desired update of EZ_1 is effected with

$$EZ_1^{n+1}=EZ_1^n+\frac{\Delta t}{\epsilon}\frac{\partial HY}{\partial x}^{n+1/2}_{i=1}. \qquad (14)$$

In Section 3.1 we show the necessary stability condition also holds for this case, and provide a two-dimensional numerical test employing this procedure in Section 5.1.

3.1. *Stability*

A standard Von Neumann analysis of (4) and (5) on an unbounded uniform Cartesian grid with mesh size h results in the well-known CFL stability condition

$$\frac{\Delta t}{\sqrt{\min\{\epsilon \cdot \mu\}}} \leq \frac{h}{\sqrt{d}},$$

where d is the number of spatial dimensions [3]. The application of boundary conditions on electric field grid points does not alter the stability condition. When dielectrics are present, one first determines the maximum h for accuracy by using the max $\{\epsilon \cdot \mu\}$ over the domain of interest and the maximum frequency to be resolved with a preset number of points per wavelength; the stability condition then sets the maximum allowed time step for that particular h.

A similar analysis for (4) and (6) on an unbounded uniform Cartesian grid with mesh size h results in the CFL condition

$$\frac{\Delta t}{\sqrt{\min\{\epsilon \cdot \mu\}}} \leq 2\frac{h}{\rho^{\infty}} \text{ [5]},$$

where ρ^{∞} is the spectral radius of the matrices used to compute spatial derivatives; for the differentiation matrix scaled by h, it is $\rho^{\infty} = \frac{7}{3}\sqrt{d}$. In this paper we consider (10) for $d = 1, 2, 3$, and the following eigenvalue analysis verifies that the same necessary condition holds for stability over bounded domains; we do not prove herein that this condition is also sufficient for stability.

First, we analyze the stability of the $d = 1$ semi-discrete versions of (10) ($\Delta t \to 0$ for a fixed $h \neq 0$) on a bounded domain in order to determine whether the inclusion of the one-sided differencing operators and the imposition of boundary conditions result in a stable scheme. We will do so by neglecting the $[HX]$ grid function, setting $h = \Delta x$, $\epsilon = \mu = 1$, and considering the system

$$\frac{d\mathbf{u}}{dt} = \frac{1}{h}\mathbf{M} \cdot \mathbf{u}. \tag{15}$$

The vector $\mathbf{u} = \{EZ_0, EZ_1, \ldots, EZ_{N-1}, EZ_N, HY_{1/2}, HY_{3/2}, \ldots, HY_{N-3/2}, HY_{N-1/2}\}$ is the solution on the grid, and $\mathbf{M}$ is the matrix composed of the difference operators represented by (8) and (9). We will consider the case in which $\mathbf{M}$ enforces homogeneous Dirichlet boundary conditions $EZ_0 = EZ_N = 0$ at the first and last (boundary) nodes of the grid. Assuming $\mathbf{u} = e^{\lambda t}\tilde{\mathbf{u}}$, where λ are the eigenvalues of $\mathbf{M}$, and $\tilde{u}$ is a complex-valued constant vector, the spectral radius of $\mathbf{M}$, provided $\Re\{\lambda\} = 0$, will be $\rho^M = \max|\Im\{\lambda\}|$, and the semi-discrete scheme will be stable. The fully discrete scheme, using staggered Leapfrog time integration and including the case $\epsilon, \mu \neq 1$, will be stable when

$$\frac{\Delta t}{\sqrt{\min\{\epsilon \cdot \mu\}}} \leq 2\frac{h}{\rho^M}. \tag{16}$$

We now show (16) is valid for a computational domain that is filled with a homogeneous dielectric and is truncated with homogeneous Dirichlet boundary conditions on the electric field. Figure 1 shows the spectral radius of $\mathbf{M}$ as a function of the mesh size; the MATLAB function *eig*, with long format, was used to compute ρ^M. We found that $\Re\{\lambda\} = O(10^{-16})$

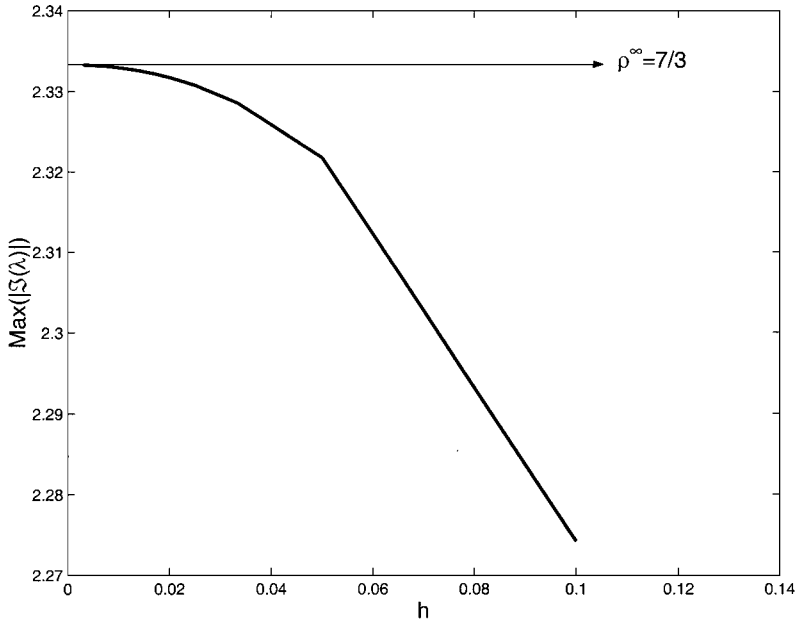

FIG. 1. The spectral radius ρ_M as a function of mesh size for Dirichlet boundary conditions.

for all h. As $h \to 0$, $\rho^M \to \rho^\infty$ from below, i.e., the explicit(2, 4) on a bounded domain is stable for the same CFL number as in an unbounded domain.

Condition (16) has also been verified for $d = 2$ by proceeding as in the one-dimensional case with **u** appropriately defined in terms of EZ, HX, HY values on a two-dimensional grid. Figure 2 shows information similar to that in Fig. 1 (we have not been able to consider

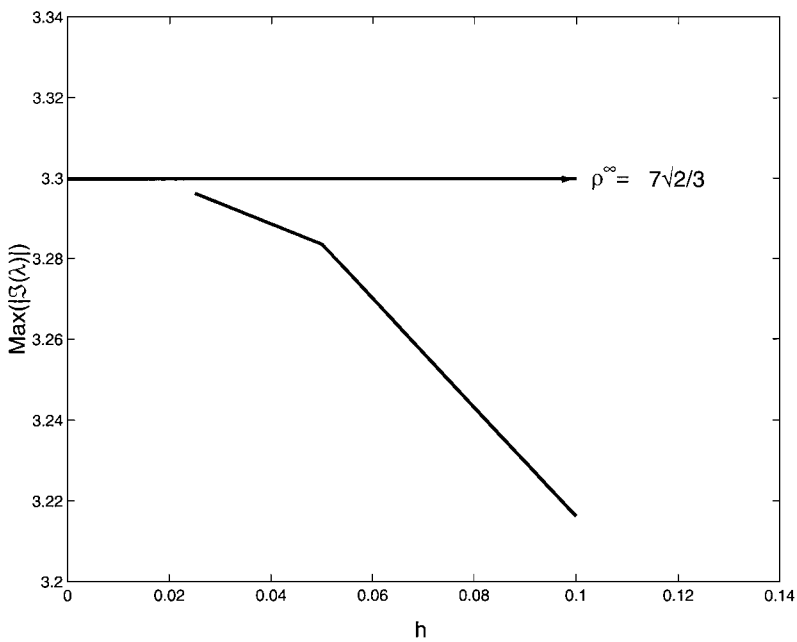

FIG. 2. Same as Fig. 1, for $d = 2$.

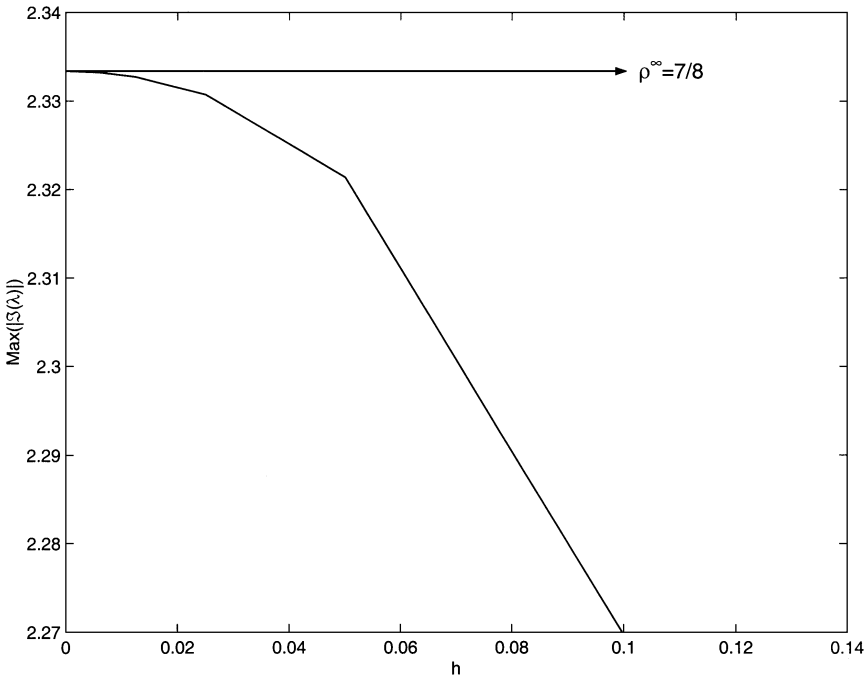

FIG. 3. Same as Fig. 1, for the PEC imposed on a tangential Magnetic field node.

smaller h values because of computer memory restrictions), and indicates that in two dimensions $\rho^M \to 7\sqrt{2}/3$ from below, i.e., the explicit(2, 4) on a bounded two-dimensional domain is stable for the same CFL number as in an unbounded domain. It was found that $\Re\{\lambda\} = O(10^{-15})$ for all h considered. In three dimensions, we have verified numerically (see last example in Section 5.1) that $\rho^M \to 7\sqrt{3}/3$.

When the PEC boundary occurs on a tangential magnetic field node, the above analysis indicates that the necessary stability condition (16) is still valid. Figure 3 shows the spectral radius of the resulting **M** as a function of the mesh size. In this case we found that $\Re\{\lambda\} = O(10^{-15})$ for h corresponding to $40 - 1280$ points per wavelength, except for $h = 1/10$ and $h = 1/20$, where $\Re\{\lambda\} = O(10^{-8})$ and $\Re\{\lambda\} = O(10^{-9})$, respectively.

4. THE SCHEME IN AN INHOMOGENEOUS BOUNDED DIELECTRIC

Consider a two-dimensional computational domain over which the dielectric permittivity is a piecewise constant function of the horizontal coordinate only, with the points of discontinuity of the material property occurring on electric field grid points. Then, we are faced with the problem of deriving finite difference expressions to correctly update the electric field on those grid points. For the sake of exposition, let $\epsilon = \epsilon_1$ to the left of the interface, and $\epsilon = \epsilon_2$ to the right, with $\mu = \mu_0$ everywhere. Across such a dielectric interface, the tangential components of the electromagnetic field, EZ and HY in this case, are continuous. Further, the first-order derivative of EZ is continuous, while that of HY is discontinuous, and second- and higher-order derivatives of both fields are discontinuous.

To implement the Yee scheme on a dielectric interface we set $\epsilon_{\text{interface}} = \frac{\epsilon_1+\epsilon_2}{2}$. This can be shown to be the appropriate material property for the grid point of discontinuity, as a local truncation error analysis indicates first-order accuracy in the mesh size; then, the global second-order convergence rate of the scheme is not affected as it is also confirmed by the numerical results. The implementation of discontinuous dielectric properties in the explicit(2, 4) via a fourth-order explicit interpolation of the dielectric permittivity on electric field nodes results, as our numerical experiments (Section 5.2) show, in a loss of two orders in the convergence rate of the explicit(2, 4). The same convergence rate reduction is obtained when the method outlined for the Yee scheme is employed to model an interface in the explicit(2, 4).

An innovative approach to handle piecewise-constant dielectric properties for the Yee scheme, when the discontinuities occur between grid points, is presented in [15, 16]. Herein, we extend this approach to include such dielectric properties in the explicit(2, 4) scheme as long as the discontinuities occur on electric field grid points. The numerical experiments in Section 5 confirm a global fourth-order convergence rate for the scheme presented below.

We present our approach for the problem of a vertical dielectric slab placed in a domain bounded on all sides by a metal. We divide the computational domain into three subdomains; two contain air, and the third one contains the lossless dielectric. Inside each subdomain, the difference equations (10) are applied to update the solution. The Dirichlet condition on the electric field is used to complete the scheme near the metal boundaries (see Section 3). The dielectric interface is also treated as a boundary point for the scheme (10) in the adjacent subdomains. Suppose those dielectric interfaces are located at $i = I_1$ and $i = I_2$, and $\epsilon = \epsilon_2$ for $I_1 < i < I_2$ while $\epsilon = \epsilon_1$ for $i > I_2$ and $i < I_1$. We need to derive difference equations to update the electric field on these boundaries (the dielectric interfaces). We assign each interface node to belong to one of the two abutting subdomains, and require that we do not difference across the jump in the material properties. In this particular case, we take $i = I_1$, I_2 to be the boundary nodes of the subdomain that is filled with the dielectric $\epsilon = \epsilon_2$. To that effect, we first approximate HY (which is continuous across the interface) at $i = I_1$ and $i = I_2$ by using the following fifth-order extrapolation with data from the subdomain that does not contain the interface node:

$$\begin{aligned} HY_{I_1,j}^{n+1/2} &= \frac{315}{128} HY_{I_1-1/2,j}^{n+1/2} - \frac{105}{32} HY_{I_1-3/2,j}^{n+1/2} + \frac{189}{64} HY_{I_1-5/2,j}^{n+1/2} \\ &\quad - \frac{45}{32} HY_{I_1-7/2,j}^{n+1/2} + \frac{35}{128} HY_{I_1-9/2,j}^{n+1/2} \\ HY_{I_2,j}^{n+1/2} &= \frac{315}{128} HY_{I_2+1/2,j}^{n+1/2} - \frac{105}{32} HY_{I_2+3/2,j}^{n+1/2} + \frac{189}{64} HY_{I_2+5/2,j}^{n+1/2} \\ &\quad - \frac{45}{32} HY_{I_2+7/2,j}^{n+1/2} + \frac{35}{128} HY_{I_2+9/2,j}^{n+1/2}. \end{aligned} \tag{17}$$

Once HY is approximated on the interface (i.e., on the boundary node), we approximate its $\hat{x}$-derivative at that location using data from the subdomain that contains the interface as

a boundary (i.e., we do not difference across interfaces) as follows:

$$\begin{aligned}\Delta x\frac{\partial}{\partial x}HY^{n+1/2}_{I_1,j} &= -\frac{1126}{315}HY^{n+1/2}_{I_1,j}+\frac{315}{64}HY^{n+1/2}_{I_1+1/2}-\frac{35}{16}HY^{n+1/2}_{I_1+3/2,j}\\ &\quad+\frac{189}{160}HY^{n+1/2}_{I_1+5/2,j}-\frac{45}{112}HY^{n+1/2}_{I_1+7/2,j}+\frac{35}{576}HY^{n+1/2}_{I_1+9/2,j}\\ \Delta x\frac{\partial}{\partial x}HY^{n+1/2}_{I_2,j} &= \frac{1126}{315}HY^{n+1/2}_{I_2,j}-\frac{315}{64}HY^{n+1/2}_{I_2-1/2}+\frac{35}{16}HY^{n+1/2}_{I_2-3/2,j}\\ &\quad-\frac{189}{160}HY^{n+1/2}_{I_2-5/2,j}+\frac{45}{112}HY^{n+1/2}_{I_2-7/2,j}-\frac{35}{576}HY^{n+1/2}_{I_2-9/2,j}.\end{aligned}\tag{18}$$

Once $\frac{\partial}{\partial x}HY^{n+1/2}_{I_1,j}$ and $\frac{\partial}{\partial x}HY^{n+1/2}_{I_2,j}$ are calculated, we update the electric field on the interfaces by evaluating $EZ^{n+1}_{I_1,j}$ and $EZ^{n+1}_{I_2,j}$ in the following way, e.g., at $i=I_1$:

$$\begin{aligned}EZ^{n+1}_{I_1,j} &= EZ^{n}_{I_1,j}-\frac{\Delta t}{\epsilon_2 24\Delta y}\left(HX^{n+1/2}_{I_1,j-3/2}-27HX^{n+1/2}_{I_1,j-1/2}+27HX^{n+1/2}_{I_1,j+1/2}-HX^{n+1/2}_{I_1,j+3/2}\right)\\ &\quad+\frac{\Delta t}{\epsilon_2}\frac{\partial}{\partial x}HY^{n+1/2}_{I_1,j}.\end{aligned}\tag{19}$$

Similarly, at $i=I_2$ to update $EZ^{n+1}_{I_2,j}$.

For a given dielectric contrast we found that differencing inside the subdomain (while extrapolating to the interface the field variable to be differenced using data from outside the subdomain) with the smaller dielectric constant results in a slight improvement of the error. Also, we observed that this improvement is lost for large contrast, and therefore concluded that it does not, in general, matter which subdomain we choose inside which do difference. This is because higher contrasts imply a larger loss of smoothness across the dielectric interface and a consequent increase of the local error.

If the dielectric interface is located at $i=I_1+1/2$, where a tangential magnetic field is collocated, the treatment differs slightly from that given above. Now, EZ and HY exchange roles. We first extrapolate EZ to the interface (using data outside the subdomain that contains the interface)

$$\begin{aligned}EZ^{n}_{I_1+1/2,j} &= \frac{315}{128}EZ^{n}_{I_1,j}-\frac{105}{32}EZ^{n}_{I_1-1,j}+\frac{189}{64}EZ^{n}_{I_1-2,j}\\ &\quad-\frac{45}{32}EZ^{n}_{I_1-3,j}+\frac{35}{128}EZ^{n}_{I_1-4,j},\end{aligned}$$

and then approximate the x derivative of EZ at that location (using data from the subdomain that contains the interface as a boundary)

$$\begin{aligned}\Delta x\frac{\partial}{\partial x}EZ^{n}_{I_1+1/2,j} &= -\frac{1126}{315}EZ^{n}_{I_1+1/2,j}+\frac{315}{64}EZ^{n}_{I_1+1,j}-\frac{35}{16}EZ^{n}_{I_1+2,j}\\ &\quad+\frac{189}{160}EZ^{n}_{I_1+3,j}-\frac{45}{112}EZ^{n}_{I_1+4,j}+\frac{35}{576}EZ^{n}_{I_1+5,j}.\end{aligned}$$

Finally, we update the magnetic field at $i=I_1+1/2$ with

$$HY^{n+1/2}_{I_1+1/2,j}=HY^{n-1/2}_{I_1+1/2,j}+\frac{\Delta t}{\mu}\frac{\partial}{\partial x}EZ^{n}_{I_1+1/2,j}.$$

We do not pursue this case any further in the present paper.

4.1. *Stability*

A stability analysis is now given for the semi-discrete version of (10) ($\Delta t \to 0$ for a fixed $h \neq 0$). Again, we consider a one-dimensional ($d = 1$) bounded domain separated in two halves by a dielectric interface at the electric field grid point $I = I_{int}$. We neglect the $[HX]$ grid function, set $h = \Delta x$, $\epsilon = \mu = 1$ for grid points $i < I_{int}$ and $\epsilon = \epsilon_2$ for grid points $i \geq I_{int}$, and consider the system

$$\frac{d\mathbf{u}}{dt} = \frac{1}{h}\mathbf{M_d} \cdot \mathbf{u}, \tag{20}$$

where $\mathbf{u} = \{EZ_0, EZ_1, \ldots, EZ_{N-1}, EZ_N, HY_{1/2}, HY_{3/2}, \ldots, HY_{N-3/2}, HY_{N-1/2}\}$ is the solution vector on the grid, and $\mathbf{M_d}$ is the matrix composed of the difference operators represented by (8), (9), and (17)–(19). Again, we consider the case in which $\mathbf{M}$ enforces homogeneous Dirichlet boundary conditions $EZ_0 = EZ_N = 0$ at the first and last (boundary) nodes of the grid. As in Section 3.2, if the eigenvalues λ of $\mathbf{M_d}$ are such that $\Re\{\lambda\} = 0$, the spectral radius of $\mathbf{M_d}$ will be $\rho^{M_d} = \max|\Im\{\lambda\}|$, and then the semi-discrete scheme will be stable. Consequently, a necessary (again, not sufficient) stability condition for the fully discrete scheme (including the case $\epsilon, \mu \neq 1$) is (16) with $\rho^M = \rho^{M_d}$.

Figure 4 shows the spectral radius of $\mathbf{M_d}$ as a function of mesh size h, and of the contrast $\epsilon = \epsilon_2/\epsilon_1$. Again, we determined that $\Re\{\lambda\} = O(10^{-16})$ for all h and ϵ of interest.

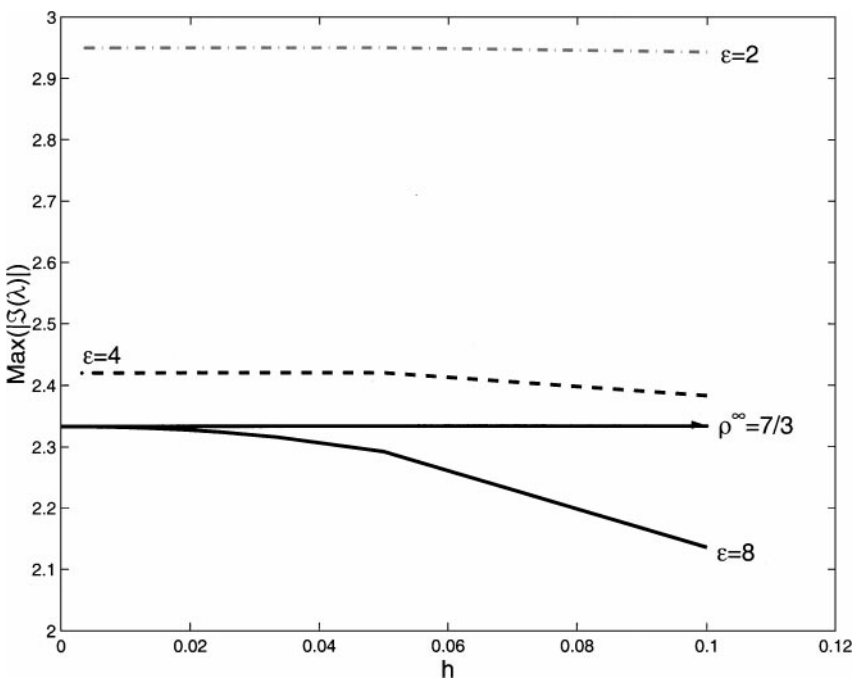

FIG. 4. The spectral radius ρ_M as a function of mesh size for the symmetric scheme with Dirichlet boundary conditions and a dielectric interface ($\Re\{\lambda\} = O(10^{-16})$).

However, as the figure shows, the maximum allowed CFL number is now smaller than that obtained in Section 3.2 because the value of ρ^{M_d}, when $h \to 0$, depends on ϵ and can be greater than ρ^{∞} for some ϵ. We note that for a given ϵ, ρ^{M_d} again approaches a limit from below as $h \to 0$. Therefore, in this case, we can only say that the interface treatment is stable and, in general, requires a slight reduction of the maximum allowed time step (for a given h). This is not restrictive for the model scheme considered herein as one would run it with a small CFL number in order to obtain fourth-order accurate results. The stability condition for dielectrics has been verified numerically for $d = 1, 2$.

The decision to approximate $\frac{\partial}{\partial x} HY_{i,j}^{n+1/2}$, when the grid point (i, j) is on a dielectric interface, with a symmetric formula (symmetric in the sense that an equal number of grid points to the left and right of an interface are to be used) was arrived at after some numerical experimentation. We initially considered asymmetric formulas, and found that they are to be avoided, as the asymmetry introduces a long-time instability for some values of h. For example, Fig. 5 shows the maximum and minimum values of $\Re\{\lambda\}$ as a function of the mesh size h when $\epsilon = 4$ (similar results were obtained for other values of the dielectric contrast). Now, $\Re\{\lambda\} = 0$ for some h. A computational test with an h for which $\Re\{\lambda\} \approx 3 \times 10^{-3}$ was unstable after 800 time units. Based on the eigenvalue analysis, the time to instability for this example was approximately 333 time units; we attribute the observed delay to the presence of eigenvalues with $\Re\{\lambda\} < 0$ of approximately the same magnitude at the given h and ϵ.

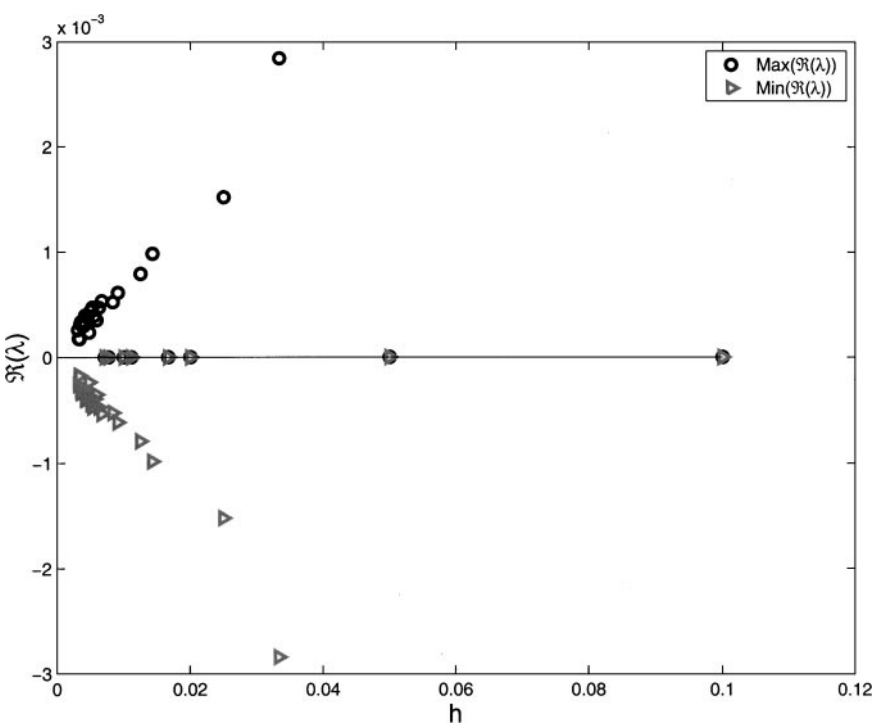

FIG. 5. $\Re\{\lambda\}$ as a function of mesh size for the non-symmetric scheme with Dirichlet boundary conditions and a dielectric interface with $\epsilon = 4$.

5. COMPUTATIONAL RESULTS

This section provides numerical tests of the boundary/interface treatment for the explicit(2, 4). At the same time we compare the results to those obtained with the Yee scheme, and, when available, to those obtained with the compact-implicit Ty(2, 4) scheme [10]. All three schemes are advanced in time by the $O(\Delta t^2)$-accurate staggered leapfrog method, and a uniform grid spacing is employed. For all computations (except one, which models the transverse electric case) we choose $\mu = 1$ everywhere, and $\epsilon = 1$ for grid points in empty space, while $\epsilon > 1$ for grid points inside a dielectric medium. In all our tests, metal boundaries and dielectric interfaces occur on electric field grid points. When presented, the error is measured against the exact solution for E_z in the L_2 norm over space (except in example two in Section 5.3, where the error is measured in the L_∞ norm over a plane curve). We also provide tables of the error in the L_∞ norm over a fixed time interval for the purpose of deducing convergence rates. For the examples posed in an open domain, we restrict the time interval over which we measure the error so that our computed results are not contaminated by reflections from the far-field boundary treatment. All examples in Sections 5.1–5.3 were coded in MATLAB.

5.1. *Closed Homogeneous Domains*

We begin with an example of engineering interest. Because of the ease of meshing geometries that conform to a Cartesian mesh, the Yee scheme is often used to compute the resonant frequencies of structures in microwave circuitry, e.g., cavities. This is accomplished by exciting a spatial point in the cavity (herein we do so with a Kronecker delta-function in space and time), and recording the time-domain solution at another location for a certain amount of time units. The resonant frequencies of the cavity (up to the frequency for which there is enough resolution) will then be the locations of the peaks of the magnitude of the Fourier transform of the recorded time-domain solution. In our example, the obtained spectra were individually scaled for graphical purposes. We applied the Yee scheme to compute the first five resonances of a $[0, 1] \times [0, 1]$ cavity with PEC walls ($E_z = 0$ there). With $\Delta t = 2h/3$, the results converged after $h = 1/40$. The decision to consider a result as "converged" was taken by running the Yee scheme for $h = 1/10, 1/20, 1/40, 1/80, 1/160$ and finding the resolution past which a refinement of the grid did not affect the positions of the first five peaks of the spectrum of the cavity. We found the $h = 1/40$ result to have "converged;" that required running the $h = 1/80$ case also. The number of time steps for $h = 1/40$ and $h = 1/80$ were 4096 and 8192, respectively. We then run the explicit(2,4) for the same h as the Yee scheme but with $\Delta t = h^2$, and the $h = 1/10$ computation required 6826 time steps to record the solution in the same time interval as for the Yee scheme. We found the locations of the first five resonances of the cavity computed with $h = 1/10$ did not shift with higher resolution. Figure 6 indicates that using the explicit(2, 4) scheme results in a 16-fold savings in memory while requiring only $2/3$ more time steps than the Yee scheme.

Using the geometry of the previous example we now consider the case in which PEC is located on tangential magnetic field nodes; now $\partial H_x/\partial y = 0$ and $x = 0, 1$ and $\partial H_y/\partial x = 0$ at $y = 0, 1$. The scheme is again (10) but with (8) and (9) altered to implement the boundary closure described by (13) and (14). Figure 7 shows the actual logarithmic errors as a function of time measured against an exact solution and indicates a slightly better than fourth-order convergence rate over the time interval considered.

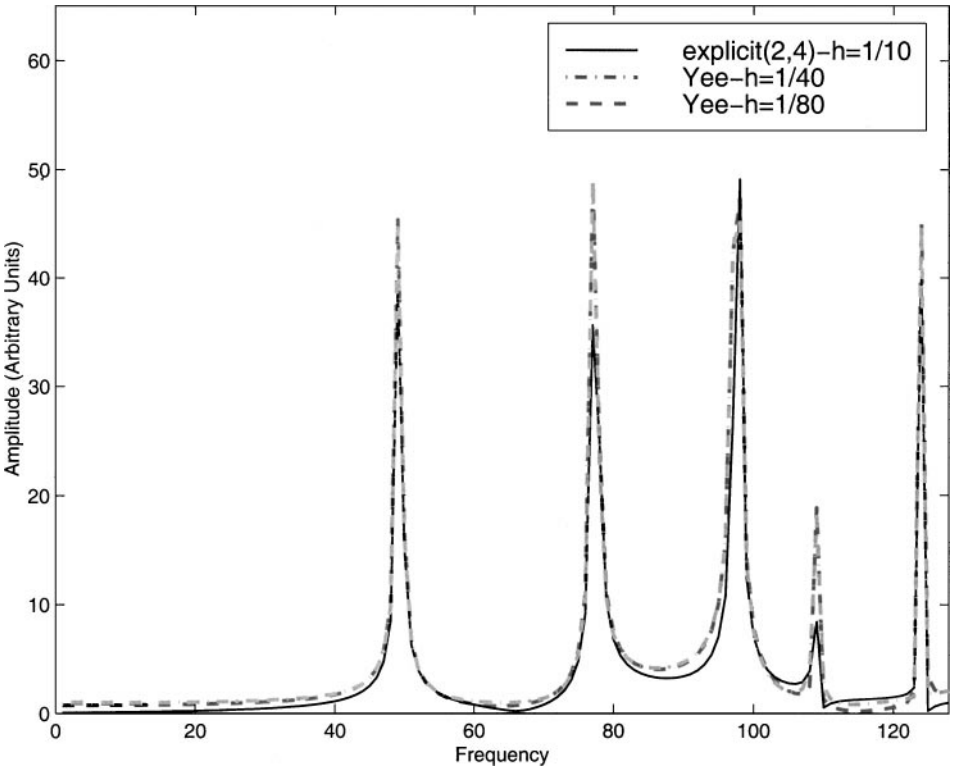

FIG. 6. The first 5 resonances of a square cavity with PEC walls.

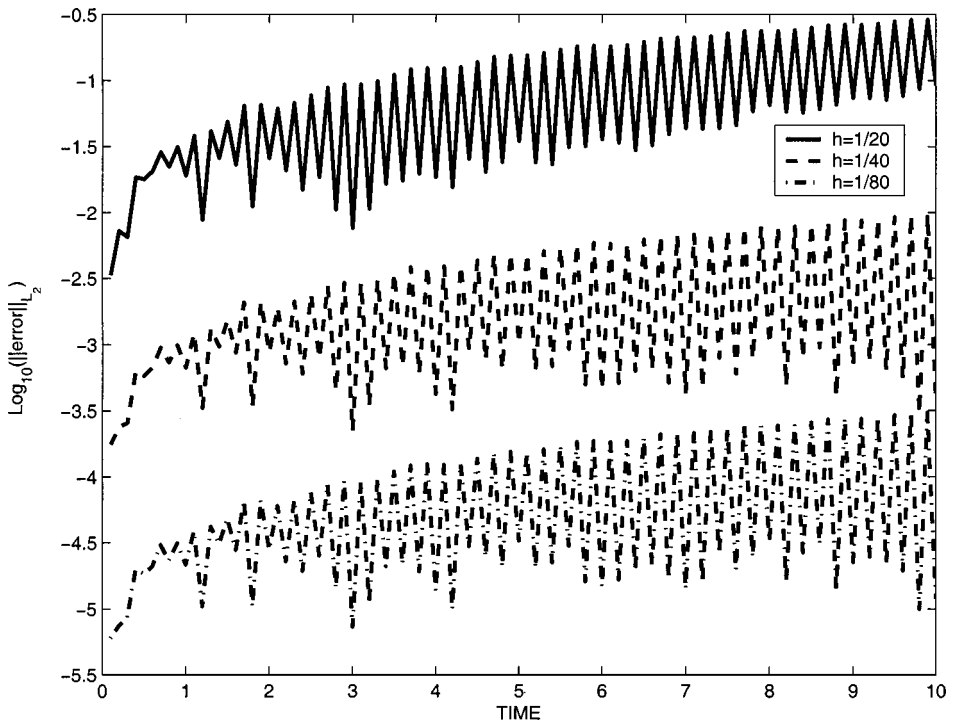

FIG. 7. $\log_{10}(\|error\|_{L_2})$ for the explicit(2, 4) scheme when the PEC is located on tangential Magentic field nodes.

We next consider single-mode propagation in a rectangular cross-section waveguide with perfectly conducting walls. We prescribe initial and boundary conditions,

$$
\begin{aligned}
E_z(x, y, 0) &= \sin(3\pi x)\sin(4\pi y),\\
H_y\left(x, y, \frac{\Delta t}{2}\right) &= -\frac{3}{5}\sin\left(3\pi x - \frac{5\pi\,\Delta t}{2}\right)\sin(4\pi y),\\
H_x\left(x, y, \frac{\Delta t}{2}\right) &= -\frac{4}{5}\cos\left(3\pi x - \frac{5\pi\,\Delta t}{2}\right)\sin(4\pi y),\\
E_z(0, y, t) &= -\sin(5\pi t)\sin(4\pi y),\\
E_z(1, y, t) &= \sin(3\pi - 5\pi t)\sin(4\pi y),\\
E_z(x, 0, t) &= 0,\\
E_z(x, 1, t) &= 0,
\end{aligned}
$$

so the exact solution is

$$E_z(x, y, t) = \sin(3\pi x - 5\pi t)\sin(4\pi y).$$

The discretization and the computational time interval is given in Table I where the convergence rates of the schemes are summarized; as the mesh is refined, the Yee scheme yields second order accuracy, while the explicit(2, 4) and Ty(2, 4) schemes yield between fourth- and fifth-order accuracy which converges to fourth-order on very fine meshes.

Finally, we test the boundary treatment by solving a three-dimensional problem over a $[0, 1/2] \times [0, 1/4] \times [0, 1/2]$ domain. An exact solution is

$$
\begin{aligned}
H_x &= \sin(\omega t)\sin(Ax + By + Cz),\\
H_y &= \sin(\omega t)\sin(Ax + By + Cz),\\
H_z &= \sin(\omega t)\sin(Ax + By + Cz),\\
E_x &= \frac{C - B}{\omega}\cos(\omega t)\cos(Ax + By + Cz),
\end{aligned}
$$

TABLE I
The Maximal Errors in L_2 Norm; Two Dimensions

Scheme	h	Δt	Max($\|\text{error}\|_{L_2}$) $0 \le t \le 10$	Rate
explicit(2, 4)	$\frac{1}{20}$	$\frac{1}{400}$	0.014	
explicit(2, 4)	$\frac{1}{40}$	$\frac{1}{1600}$	1.9316×10^{-4}	6.2
explicit(2, 4)	$\frac{1}{80}$	$\frac{1}{3200}$	6.48×10^{-6}	4.896
Ty(2, 4)	$\frac{1}{20}$	$\frac{1}{400}$	0.0242	
Ty(2, 4)	$\frac{1}{40}$	$\frac{1}{1440}$	7.9304×10^{-5}	8.15
Ty(2, 4)	$\frac{1}{80}$	$\frac{1}{3440}$	2.329×10^{-6}	5.089
Yee	$\frac{1}{20}$	$\frac{1}{30}$	0.1889	
Yee	$\frac{1}{40}$	$\frac{1}{60}$	0.0476	1.9885
Yee	$\frac{1}{80}$	$\frac{1}{120}$	0.0119	2.0032

TABLE II
The Maximal Errors in L_2 Norm; Three Dimensions

Scheme	h	Δt	Max($\|\text{error}\|_{L_2}$) $0 \le t \le 10$	Rate
explicit(2, 4)	$\frac{1}{20}$	$\frac{1}{400}$	5.375×10^{-4}	
explicit(2, 4)	$\frac{1}{40}$	$\frac{1}{1600}$	2.184×10^{-5}	4.621
explicit(2, 4)	$\frac{1}{80}$	$\frac{1}{3200}$	9.071×10^{-7}	4.590
Ty(2, 4)	$\frac{1}{20}$	$\frac{1}{400}$	3.621×10^{-4}	
Ty(2, 4)	$\frac{1}{40}$	$\frac{1}{1600}$	1.144×10^{-5}	4.983
Ty(2, 4)	$\frac{1}{80}$	$\frac{1}{6400}$	3.5621×10^{-7}	5.005
Yee	$\frac{1}{20}$	$\frac{1}{35}$	0.0027	
Yee	$\frac{1}{40}$	$\frac{1}{70}$	7.3×10^{-4}	1.9028
Yee	$\frac{1}{80}$	$\frac{1}{140}$	1.8252×10^{-4}	2.0015

$$E_y = \frac{A - C}{\omega} \cos(\omega t) \cos(Ax + By + Cz),$$
$$E_z = \frac{B - A}{\omega} \cos(\omega t) \cos(Ax + By + Cz),$$

where $\omega^2 = A^2 + B^2 + C^2$ and $A + B + C = 0$ with $A = \pi$, $B = -2\pi$, $C = \pi$, and $\omega = \sqrt{6}\pi$. Table II shows that the (2, 4) schemes outperform the Yee scheme by being more accurate, and by exhibiting higher-order convergence rates. We found the scheme is unstable for $CFL > 7\sqrt{3}/3$.

5.2. *Closed Inhomogeneous Domains*

Let a domain which contains air and a lossless dielectric with a relative permittivity of ϵ_2 be as shown in Fig. 8. For the Yee scheme we will use the arithmetic average of the permittivity on electric field nodes on the interface, while for the (2, 4) schemes we will first use a fourth-order interpolation for ϵ and then our new treatment given in Section 4. An exact solution for time-varying electromagntic fields in such a

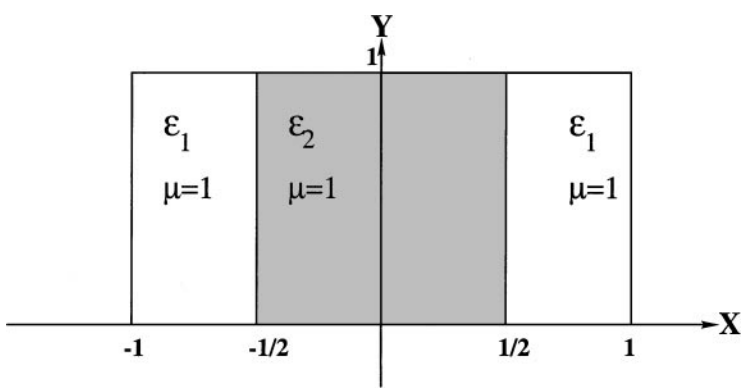

FIG. 8. The computational domain.

TABLE III
The Maximal Errors in L_2 Norm with $\epsilon_2 = 2$

Scheme	h	Δt	Max($\|\text{error}\|_{L_2}$) $0 \le t \le 10$	Rate
explicit(2, 4)	$\frac{1}{20}$	$\frac{1}{400}$	0.0019	
explicit(2, 4)	$\frac{1}{40}$	$\frac{1}{1600}$	5.7585×10^{-4}	1.715
explicit (2, 4)	$\frac{1}{80}$	$\frac{1}{3200}$	1.4909×10^{-4}	1.94
Ty(2, 4)	$\frac{1}{20}$	$\frac{1}{400}$	0.00196	
Ty(2, 4)	$\frac{1}{40}$	$\frac{1}{1600}$	5.7721×10^{-4}	1.763
Ty(2, 4)	$\frac{1}{80}$	$\frac{1}{6400}$	1.4995×10^{-4}	1.948
Yee	$\frac{1}{20}$	$\frac{1}{30}$	0.0363	
Yee	$\frac{1}{40}$	$\frac{1}{60}$	0.0089	2.028
Yee	$\frac{1}{80}$	$\frac{1}{120}$	0.00222	2.003

domain is

$$E_z = \begin{cases} 2\cos\left(\frac{2\pi}{3}X\right)\cos(\omega t)\sin(K_y Y) & |X| \le \frac{1}{2} \quad 0 \le Y \le 1 \\ \exp\left(\frac{\pi\sqrt{3}}{3}\right)\exp\left(-\frac{2\pi\sqrt{3}}{3}|X|\right)\cos(\omega t)\sin(K_y Y) & |X| \ge \frac{1}{2} \quad 0 \le Y \le 1 \end{cases}$$

$$H_y = \begin{cases} -\sqrt{\epsilon_2 - \epsilon_1}\sin\left(\frac{2\pi}{3}X\right)\sin(\omega t)\sin(K_y Y) & |X| \le \frac{1}{2} \quad 0 \le Y \le 1 \\ -\frac{\sqrt{3(\epsilon_2-\epsilon_1)}}{2}\exp\left(\frac{\pi\sqrt{3}}{3}\right)\exp\left(-\frac{2\pi\sqrt{3}}{3}X\right)\sin(\omega t)\sin(K_y Y) & X \ge \frac{1}{2} \quad 0 \le Y \le 1 \\ \frac{\sqrt{3(\epsilon_2-\epsilon_1)}}{2}\exp\left(\frac{\pi\sqrt{3}}{3}\right)\exp\left(\frac{2\pi\sqrt{3}}{3}X\right)\sin(\omega t)\sin(K_y Y) & X \le -\frac{1}{2} \quad 0 \le Y \le 1 \end{cases}$$

$$H_x = \begin{cases} -\sqrt{\epsilon_1 + 3\epsilon_2}\cos\left(\frac{2\pi}{3}X\right)\sin(\omega t)\cos(K_y Y) & |X| \le \frac{1}{2} \quad 0 \le Y \le 1 \\ -\frac{\sqrt{\epsilon_1+3\epsilon_2}}{2}\exp\left(\frac{\pi\sqrt{3}}{3}\right)\exp\left(-\frac{2\pi\sqrt{3}}{3}|X|\right)\sin(\omega t)\cos(K_y Y) & |X| \ge \frac{1}{2} \quad 0 \le Y \le 1, \end{cases}$$

where $K_y = \frac{2\pi}{3}\sqrt{\frac{\epsilon_1+3\epsilon_2}{\epsilon_2-\epsilon_1}}$ and $\omega = \frac{4\pi}{3\sqrt{\epsilon_2-\epsilon_1}}$. We will compare the schemes herein for $\epsilon_1 = 1$ and $\epsilon_2 = 2, 4$, using the same mesh sizes and time steps as before. Tables III and IV indicate the expected reduction of the convergence rate for the (2, 4) schemes, and the expected second-order convergence rate for the Yee scheme. Although we obtain only second-order convergence for the (2, 4) schemes, the results are better than those obtained

TABLE IV
The Maximal Errors in L_2 Norm with $\epsilon_2 = 4$

Scheme	h	Δt	Max($\|\text{error}\|_{L_2}$) $0 \le t \le 10$	Rate
explicit(2, 4)	$\frac{1}{20}$	$\frac{1}{400}$	0.0014	
explicit(2, 4)	$\frac{1}{40}$	$\frac{1}{1600}$	3.765×10^{-4}	1.894
explicit(2, 4)	$\frac{1}{80}$	$\frac{1}{3200}$	9.7748×10^{-5}	1.945
Ty(2, 4)	$\frac{1}{20}$	$\frac{1}{400}$	0.00139	
Ty(2, 4)	$\frac{1}{40}$	$\frac{1}{1600}$	3.756×10^{-4}	1.887
Ty(2, 4)	$\frac{1}{80}$	$\frac{1}{6400}$	9.7579×10^{-5}	1.944
Yee	$\frac{1}{20}$	$\frac{1}{30}$	0.0095	
Yee	$\frac{1}{40}$	$\frac{1}{60}$	0.00237	2.003
Yee	$\frac{1}{80}$	$\frac{1}{120}$	5.9442×10^{-4}	1.9953

TABLE V
The Maximal Errors in L_2 Norm with $\epsilon_2 = 2$

Scheme	h	Δt	Max($\|\text{error}\|_{L_2}$) $0 \le t \le 10$	Rate
explicit(2, 4)	$\frac{1}{20}$	$\frac{1}{400}$	3.1868×10^{-4}	
explicit(2, 4)	$\frac{1}{40}$	$\frac{1}{1600}$	4.9822×10^{-6}	5.999
explicit(2, 4)	$\frac{1}{80}$	$\frac{1}{3200}$	2.6532×10^{-7}	4.231
Ty(2, 4)	$\frac{1}{20}$	$\frac{1}{400}$	1.978×10^{-4}	
Ty(2, 4)	$\frac{1}{40}$	$\frac{1}{1600}$	2.2368×10^{-6}	6.466
Ty(2, 4)	$\frac{1}{80}$	$\frac{1}{6400}$	3.7520×10^{-7}	2.575
Yee	$\frac{1}{20}$	$\frac{1}{30}$	0.0363	
Yee	$\frac{1}{40}$	$\frac{1}{60}$	0.0089	2.028
Yee	$\frac{1}{80}$	$\frac{1}{120}$	0.00222	2.003

with the Yee scheme. However, we are using a fourth-order scheme, and the loss of two orders of convergence in the presence of heterogeneous dielectrics is undesirable.

We repeat the previous example with a code that implements the new interface treatment presented in Section 4. Tables V and VI summarize the convergence rates, and confirm the expected recovery of global fourth-order convergence for the (2, 4) schemes.

Next, numerical evidence is presented of long-time stability of our approach by considering a problem in which a dielectric of relative permittivity ϵ_2, occupying the spatial region $[0, 1/2] \times [0, 1]$, is inserted in a PEC-bounded $[0, 5/4] \times [0, 1]$ domain. An exact solution in this case is

$$E_z = \begin{cases} \sin(a_1 X)\sin(\omega t)\sin(bY) & 0 \le X \le \frac{1}{2} \quad 0 \le Y \le 1 \\ \cos(a_2 X)\sin(\omega t)\sin(bY) & \frac{1}{2} \le X \le \frac{5}{4} \quad 0 \le Y \le 1 \end{cases}$$

$$H_y = \begin{cases} -\frac{a_1}{\omega}\cos(a_1 X)\cos(\omega t)\sin(bY) & 0 \le X \le \frac{1}{2} \quad 0 \le Y \le 1 \\ \frac{a_2}{\omega}\cos(a_2 X)\cos(\omega t)\sin(bY) & \frac{1}{2} \le X \le \frac{5}{4} \quad 0 \le Y \le 1 \end{cases}$$

$$H_x = \begin{cases} \frac{b}{\omega}\sin(a_1 X)\cos(\omega t)\cos(bY) & 0 \le X \le \frac{1}{2} \quad 0 \le Y \le 1 \\ \frac{b}{\omega}\sin(a_2 X)\cos(\omega t)\cos(bY) & \frac{1}{2} \le X \le \frac{5}{4} \quad 0 \le Y \le 1, \end{cases}$$

TABLE VI
The Maximal Errors in L_2 Norm with $\epsilon_2 = 4$

Scheme	h	Δt	Max($\|\text{error}\|_{L_2}$) $0 \le t \le 10$	Rate
explicit(2, 4)	$\frac{1}{20}$	$\frac{1}{400}$	6.9209×10^{-5}	
explicit(2, 4)	$\frac{1}{40}$	$\frac{1}{1600}$	3.5383×10^{-6}	4.289
explicit(2,4)	$\frac{1}{80}$	$\frac{1}{3200}$	2.0045×10^{-7}	4.147
Ty(2, 4)	$\frac{1}{20}$	$\frac{1}{400}$	2.6958×10^{-5}	
Ty(2, 4)	$\frac{1}{40}$	$\frac{1}{1600}$	1.2869×10^{-6}	4.3887
Ty(2, 4)	$\frac{1}{80}$	$\frac{1}{6400}$	3.2753×10^{-8}	5.291
Yee	$\frac{1}{20}$	$\frac{1}{30}$	0.0095	
Yee	$\frac{1}{40}$	$\frac{1}{60}$	0.00237	2.003
Yee	$\frac{1}{80}$	$\frac{1}{120}$	5.9442×10^{-4}	1.9953

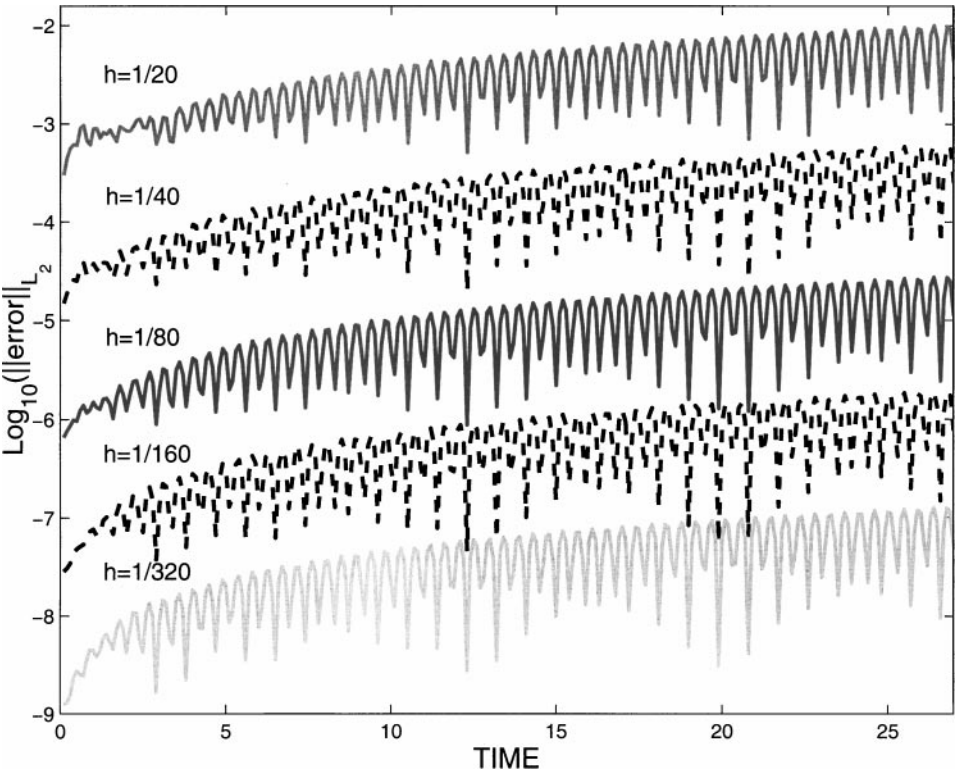

FIG. 9. $\log_{10}(\|\text{error}\|_{L_2})$ for the explicit(2, 4) scheme.

where $a_1^2 + b^2 = \epsilon_2\omega^2$, $a_2^2 + b^2 = \epsilon_1\omega^2$, $\sin(\frac{a_1}{2}) = \cos(\frac{a_2}{2})$, $\cos(\frac{5a_2}{4}) = 0$, and we choose $\epsilon_1 = 1, \epsilon_2 = 2, a_1 = 3\pi, a_2 = 2\pi, b = \pi$, and $\omega = \sqrt{5}\pi$. On the air/dielectric interface we employed the new treatment. To verify stability for a long time, we run this problem for 27 time units, with $h = 1/20, 1/40, 1/80, 1/160, 1/320$. In Fig. 9 we draw the corresponding errors as a function of time. Table VII shows the scheme remains stable and fourth-order accurate over a long-time interval.

Although in this paper we consider only the TM polarization, the applicability of our approach to the transverse electric (TE) case with a piecewise-constant ϵ (fixed μ) can be demonstrated by considering the TM equations with a piecewise-constant μ and a fixed ϵ. To that end, we coat a perfect conductor with a magnetic dielectric of thickness $\frac{1}{2}$ and

TABLE VII
The Maximal Errors in L_2 Norm with $\epsilon_2 = 2$

Scheme	h	Δt	Max($\|\text{error}\|_{L_2}$) $0 \le t \le 27$	Rate
explicit(2, 4)	$\frac{1}{20}$	$\frac{1}{400}$	0.0101	
explicit(2, 4)	$\frac{1}{40}$	$\frac{1}{1600}$	6.1264×10^{-4}	4.4815
explicit(2, 4)	$\frac{1}{80}$	$\frac{1}{3200}$	2.7431×10^{-5}	4.0428
explicit(2, 4)	$\frac{1}{160}$	$\frac{1}{3200}$	1.9041×10^{-6}	3.848
explicit(2, 4)	$\frac{1}{320}$	$\frac{1}{3200}$	1.2522×10^{-7}	3.926

TABLE VIII
The Maximal Errors in L_2 Norm with $\mu_2 = 2$

Scheme	h	Δt	Max($\|\text{error}\|_{L_2}$) $0 \le t \le 10$	Rate
explicit(2, 4)	$\frac{1}{20}$	$\frac{1}{400}$	0.0021	
explicit(2, 4)	$\frac{1}{40}$	$\frac{1}{1600}$	1.4010×10^{-4}	3.9059
explicit(2, 4)	$\frac{1}{80}$	$\frac{1}{3200}$	5.2597×10^{-6}	4.7353

relative permeability $\mu_2 = 2$ ($\mu_1 = 1$), using the geometry of the previous example. We used our interface treatment presented in Section 4, and placed the magnetic interface on an electric node. Table VIII summarizes the convergence rate and confirms our scheme's fourth-order accuracy and stability.

5.3. *Open Domains*

We consider a monochromatic isotropic point source of wavelength 0.25, that is switched on at $t = 0$ and radiates in front of an infinite perfectly conducting surface. The point source is modeled by adding a term representing a current $I_z(t) = 0.01 \sin(8\pi t) H(t)$ at $r_s = (x, y) = (\frac{1}{4}, \frac{1}{4})$, where $H(t)$ denotes the Heaviside unit-step function. For such a source, the radiated field is the solution of

$$\partial_x^2 E_z + \partial_y^2 E_z - \partial_t^2 E_z = \partial_t I_z(t) \delta\left(x - \frac{1}{4}, y - \frac{1}{4}\right). \tag{21}$$

The solution consists of rotationally symmetric outgoing waves, and is given by

$$E_z(r, t) = -\frac{1}{2\pi} \int_0^\infty \frac{\partial_t I_z(t - \sqrt{|r - r_s|^2 + \xi^2})}{\sqrt{|r - r_s|^2 + \xi^2}}\, d\xi.$$

The computational domain is $[0, \frac{1}{2}] \times [0, \frac{1}{2}]$, and the boundary condition is

$$E_z(1/2, y, t) = 0. \tag{22}$$

Because the bounding plane is infinite, the exact solution in the region of interest can be constructed by using the exact solution for (21) and the method of images, with the image source of negative strength at location $(\frac{3}{4}, \frac{1}{4})$. For the Yee scheme we choose $h = \frac{1}{40}$, $\Delta t = \frac{2h}{3}$, while for the explicit(2, 4) scheme we choose $h = \frac{1}{40}$, $\Delta t = h^2$. Figures 10–12, respectively, show the error in L_2 norm, and contour comparisons of the exact and numerical solutions. Both schemes live up to their convergence rate over domains that exclude the source region.

Our next two examples are presented in order to exemplify the type of problems that remain to be addressed. First, the source of the previous example is now considered in the presence of an inclined ($\phi = \pi/8$ with respect to the horizontal) perfectly conducting plane. The perfect conductor is staircased so that the metal boundary falls on electric field grid points, and we measure the error in the L_1 norm along the dashed line drawn in Fig. 13. Figures 14–16 show the obtained error for $h = 1/20$, $h = 1/40$, and $h = 1/80$. In this case, both the Yee and explicit(2, 4) schemes are second-order convergent as seen in Table IX.

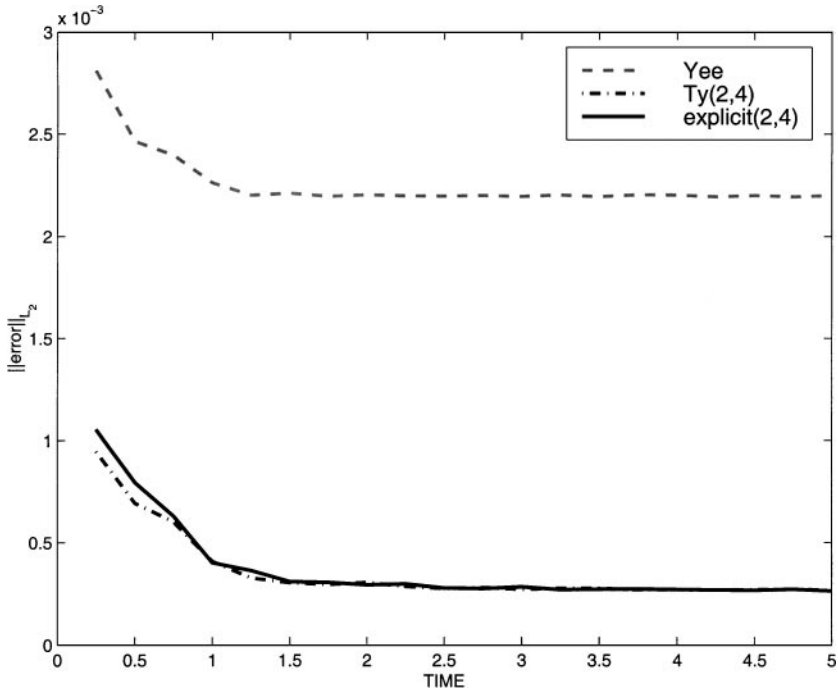

FIG. 10. $\|\text{error}\|_{L_2}$ for the mirror problem with boundary condition (22).

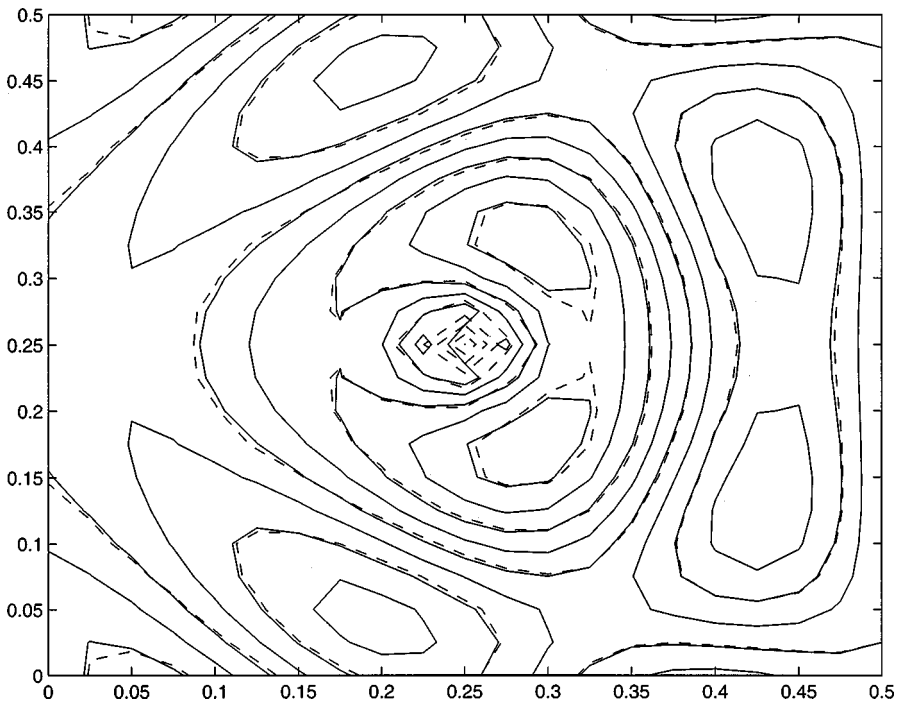

FIG. 11. Solution contours obtained with the Yee scheme ($--$), and the exact solution ($-$) at $t = 5$.

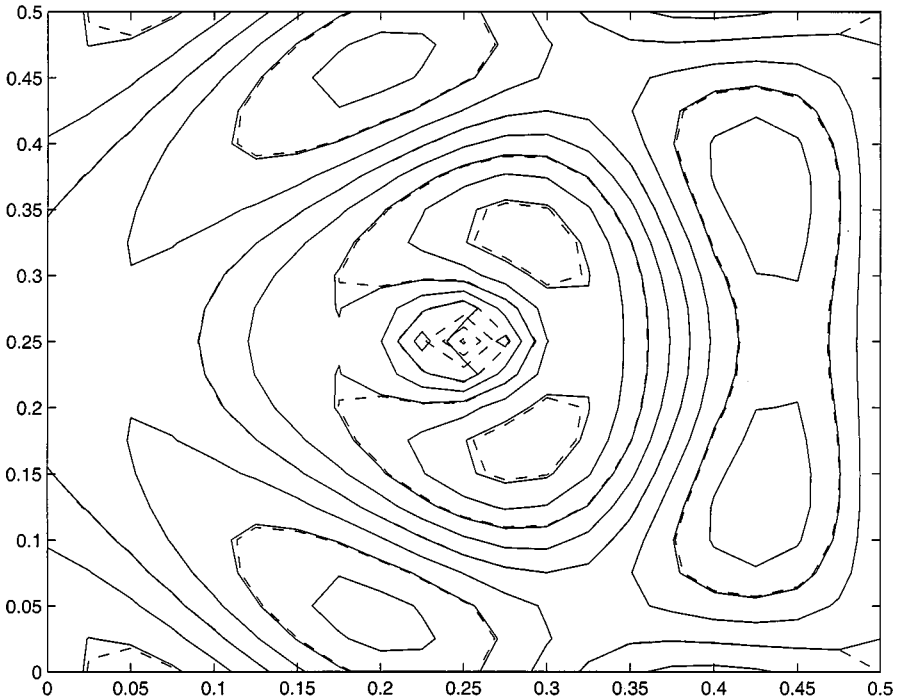

FIG. 12. Solution contours obtained with the explicit(2, 4) scheme (−−), and the exact solution (−) at $t = 5$.

This is because the local error for both schemes near the inclined plane is only first-order in the mesh size because of the artificial corners introduced by the staircasing. Figure 15 shows that the Ty(2, 4) schemes is unstable in this situation, whereas the Yee and explicit(2, 4) schemes are stable. We note here that the com Ty(2, 4) scheme [11] is stable in this situation.

Our final example involves an infinitesimally thin PEC strip illuminated by a point source as shown in Fig. 17. We implemented the dimensional form of the equations, and the spatial extend of the signal produced by the source (1.2 m) is comparable to the width of the strip (2 m). The scattered field, obtained by computing the total and incident fields and then subtracting them, was computed at locations 1 and 2 as shown in Fig. 17. Although the

TABLE IX
The Maximal Errors in L_2 Norm for the Inclined PEC Mirror

Scheme	h	Δt	Max($\|\text{error}\|_{L_2}$) $1 \le t \le 4$	Rate
explicit(2, 4)	$\frac{1}{20}$	$\frac{1}{400}$	0.0165	
explicit(2, 4)	$\frac{1}{40}$	$\frac{1}{1600}$	0.0023	2.8428
explicit(2, 4)	$\frac{1}{80}$	$\frac{1}{3200}$	4.2644×10^{-4}	2.4312
Yee	$\frac{1}{20}$	$\frac{1}{30}$	0.0359	
Yee	$\frac{1}{40}$	$\frac{1}{60}$	0.0034	3.4004
Yee	$\frac{1}{80}$	$\frac{1}{120}$	4.7338×10^{-4}	2.8445

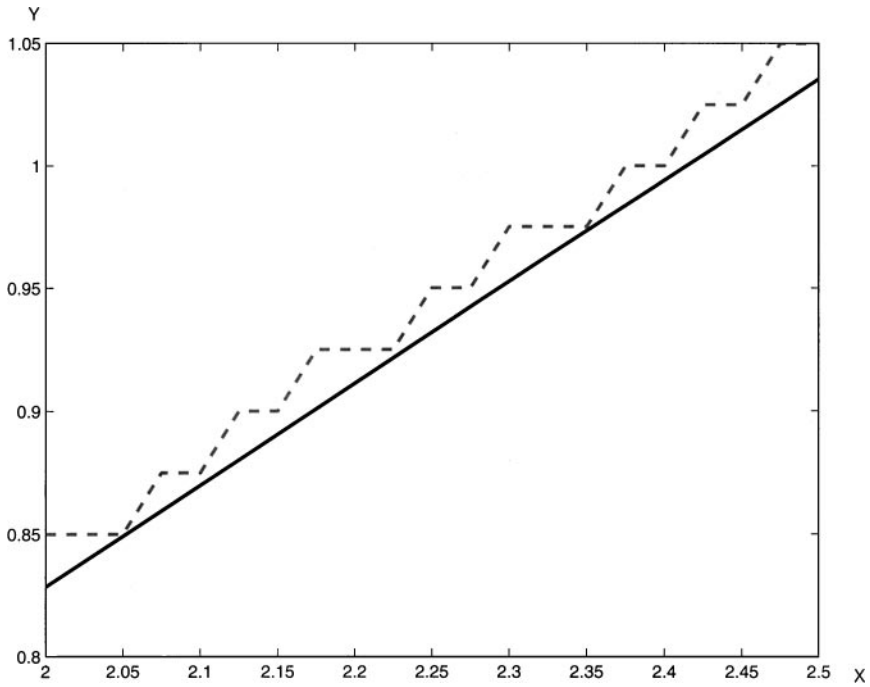

FIG. 13. Location of the grid points on which the error is measured.

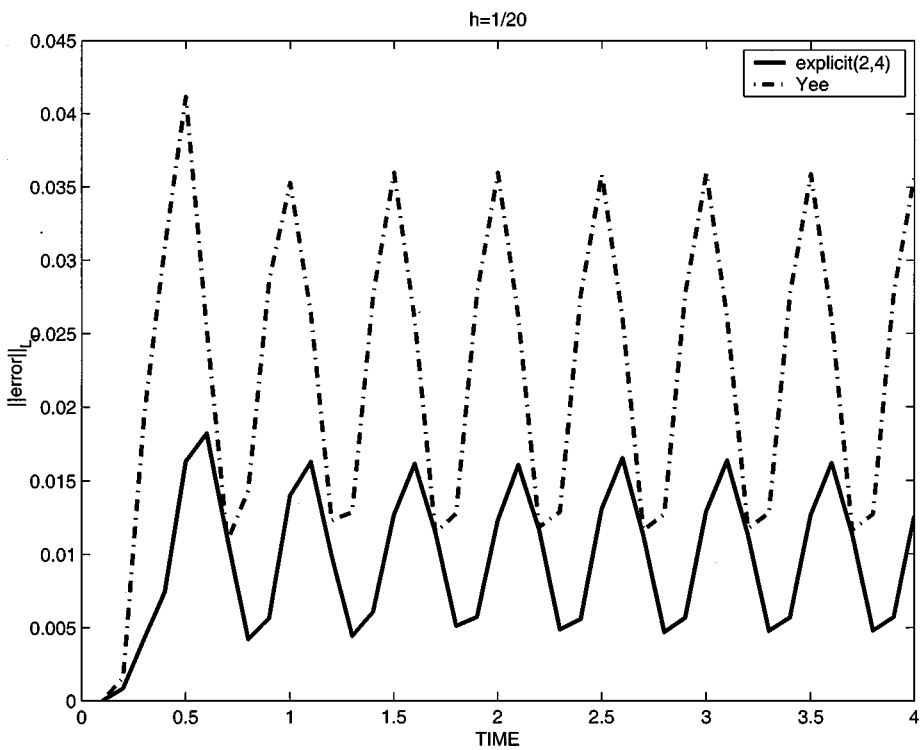

FIG. 14. $\|\text{error}\|_{L_1}$ as a function of time for the Yee and explicit(2, 4) schemes; $h = 1/20$.

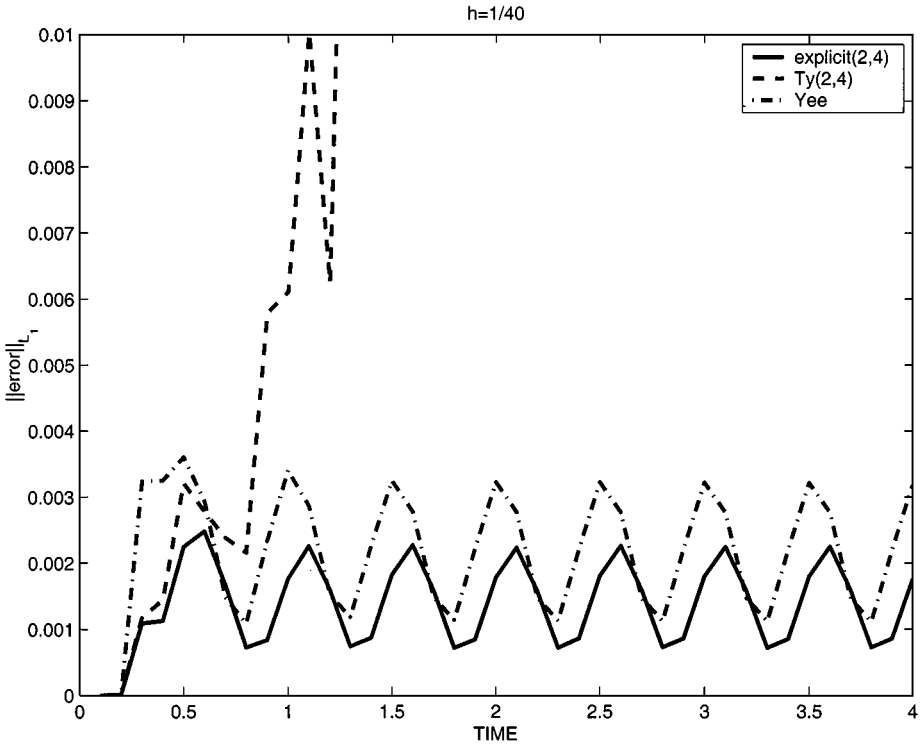

FIG. 15. $\|\text{error}\|_{L_1}$ as a function of time for the Yee, explicit(2, 4), and Ty(2, 4) schemes; $h = 1/40$.

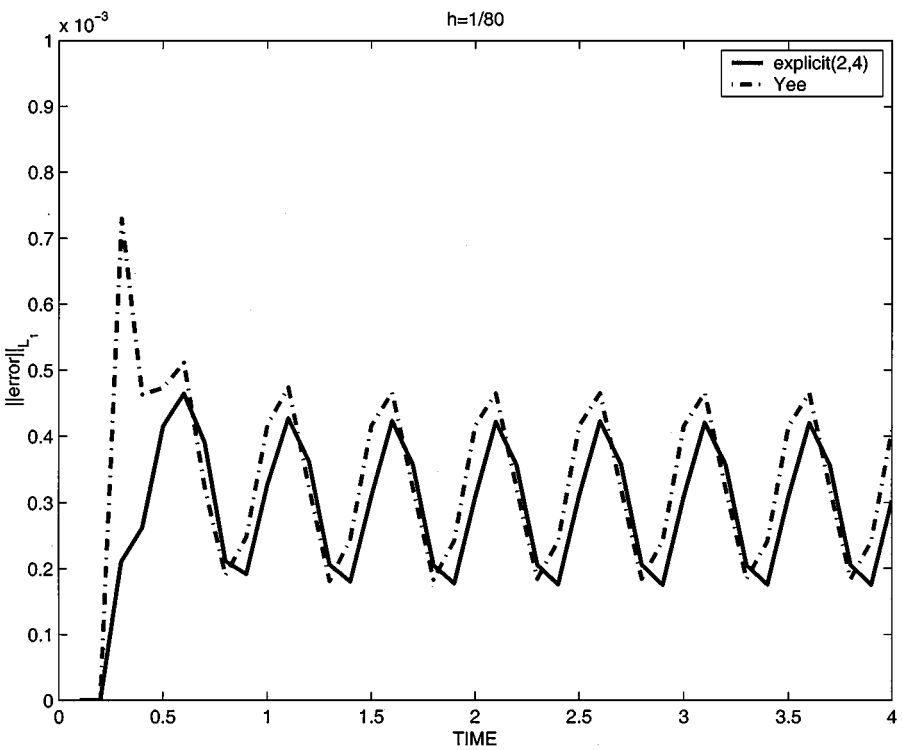

FIG. 16. $\|\text{error}\|_{L_1}$ as a function of time for the Yee and explicit(2, 4) schemes; $h = 1/80$.

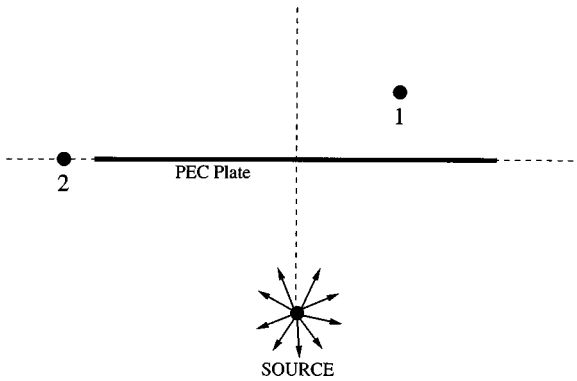

FIG. 17. Geometry of PEC strip scattering problem.

analytical solution is difficult to evaluate, we exploit the fact that the horizontal component of the scattered magnetic field is identically equal to zero outside the support of the strip [19] on the dashed line passing through location 2 in order to evaluate the performance of the high-order scheme. Figures 18 and 19 indicate that at location 1 (away from the strip) the high-order scheme produces the result obtained with the Yee scheme but with a four-times coarser grid. At the same resolution, the schemes do not completely agree (see detail in Fig. 19). At location 2 we find the fourth-order scheme gives a nonzero horizontal component for the scattered magnetic field (Fig. 20) which we determined to be first-order convergent to zero; the Yee scheme for the infinitesimally thin strip gives values consistent

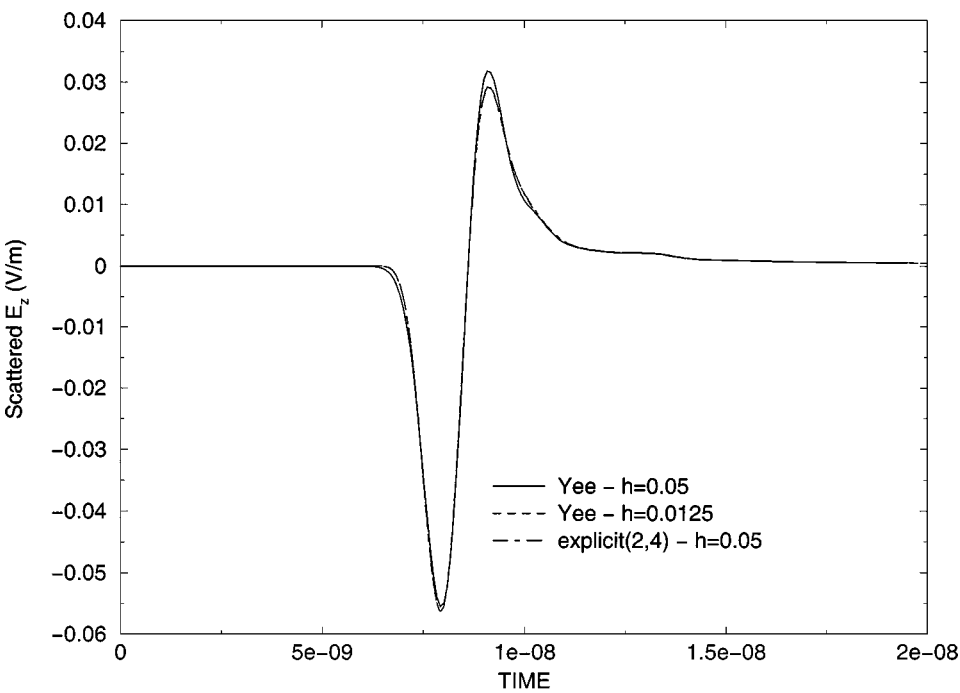

FIG. 18. Comparison of scattered E_z field at location 1.

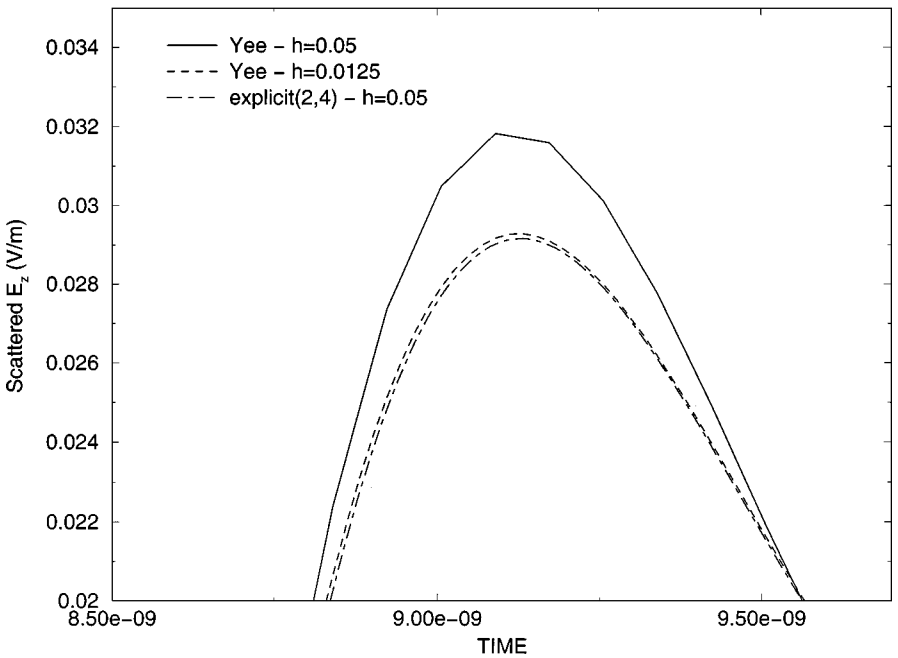

FIG. 19. Detail from Fig. 18.

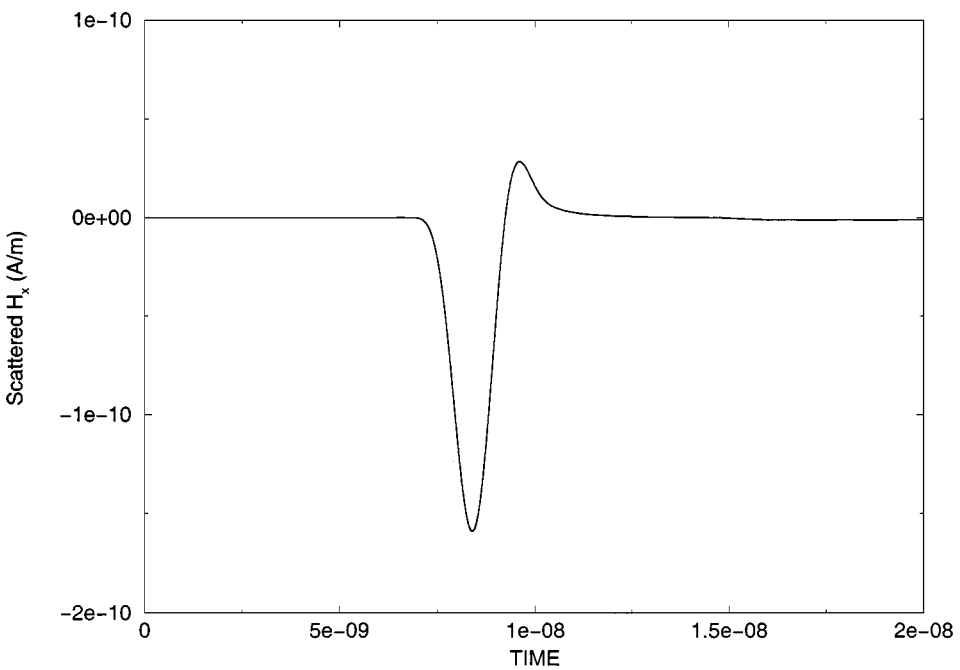

FIG. 20. Scattered H_x component at location 2 for the explicit(2, 4) scheme.

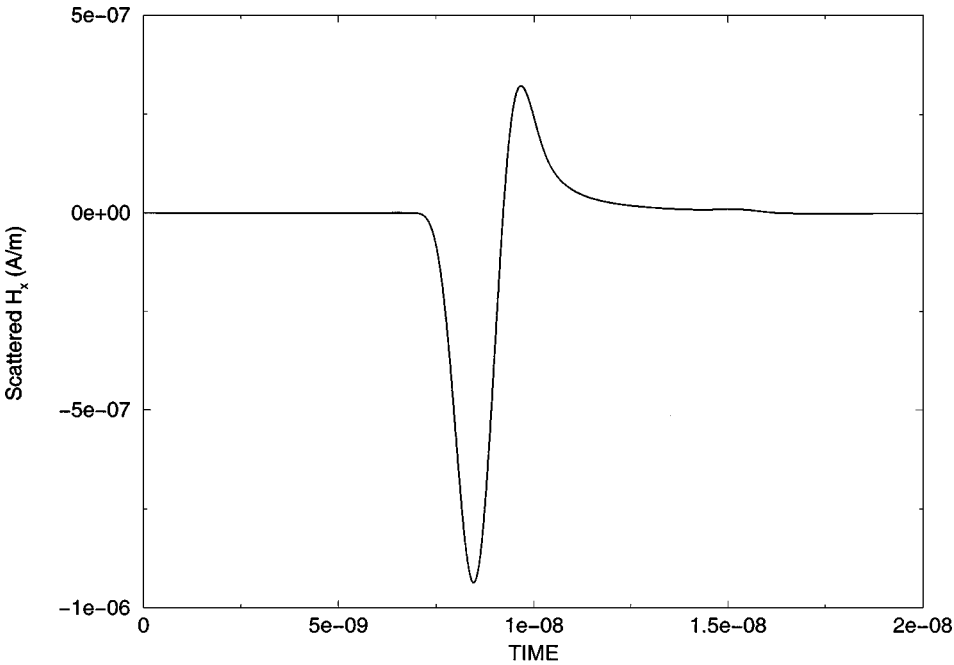

FIG. 21. Scattered H_x component at location 2 for the Yee scheme with a $2h$-thick PEC strip.

with the analytical result. We conjecture that the numerical boundary treatment surrounding the infinitesimally thin PEC strip (on which $EZ = 0$ is imposed with our approach) endows the sharp edge with an effective roundness. It is known that scattering increases when an edge is blunted [20]. We then applied the Yee scheme to the same problem but with a strip that is $2h$ thick (two rows of nodes where $(E_z = 0)$; the resemblance of the obtained result (Fig. 21) to that in Fig. 20 is offered as confirmation of our assertion.

5.4. *Relative Computational Cost*

We now compare the efficiency of the (2, 4) schemes to that of the Yee scheme by considering an empty $[0, 1] \times [0, 1]$ cavity with PEC walls excited by initial conditions. For the (2, 4) schemes we use a uniform grid spacing with $h = \Delta x = \Delta y = \frac{1}{30}$. For the Yee scheme we also use a uniform grid spacing, but with $h = \Delta x = \Delta y = \frac{1}{240}$. We chose these mesh sizes in order to obtain the same error between the exact E_z and the approximate E_z in L_2 norm. The comparison is shown in Table X. The programs were written in FORTRAN

TABLE X
CPU-Time Comparison for a Fixed Error

Scheme	h	Δt	Max($\|\text{error}\|_{L_2}$) $0 \le t \le 10$	CPU—time
explicit(2, 4)	$\frac{1}{30}$	$\frac{1}{900}$	1.99×10^{-3}	0.9 sec
Ty(2, 4)	$\frac{1}{30}$	$\frac{1}{900}$	1.25×10^{-3}	5.7 sec
Yee	$\frac{1}{240}$	$\frac{1}{360}$	1.31×10^{-3}	91 sec

and were run on a Digital 600 au Alpha workstation. We observe that the CPU time needed to achieve the same accuracy with the Yee scheme is more than 11 times larger than that required by the Ty(2, 4) scheme, and 91 times larger than that required by the explicit(2, 4) scheme. Note the time savings is realized despite the smaller time step required by the (2, 4) schemes.

6. CONCLUSION

We presented stable finite difference operators to implement boundary/interface conditions in a fourth-order accurate extension of the Yee scheme. Numerical tests confirmed that the convergence rate exhibited by the high-order scheme in the absence of boundaries is preserved in their presence; fourth-order convergence is also obtained in the presence of discontinuous electric and magnetic dielectric properties.

The results obtained in the last two examples of Section 5.3 indicate that both the boundary staircasing and the presence of geometric singularities (e.g., knife-edge) adversely affect the convergence rate. These issues are the topic of our ongoing work.

ACKNOWLEDGMENTS

This effort was sponsored by the Air Force Office of Scientific Research, Air Force Materials Command, USAF. The U.S. Government is authorized to reproduce and distribute reprints for governmental purposes notwithstanding any copyright notation thereon. The views and conclusions contained herein are those of the authors and should not be interpreted as necessarily representing the official policies or endorsements, either expressed or implied, of the Air Force Office of Scientific Research or the U.S. Government.

REFERENCES

1. A. Nachman, A brief perspective on computational electromagnetics, *J. Comput. Phys.* **129**, 237 (1996).
2. K. S. Yee, Numerical solution of initial boundary value problems involving Maxwell's equation in isotropic media, *IEEE Trans. Antennas Propagation* **14**, 302 (1966).
3. A. Taflove, *Computational Electrodynamics: The Finite-Difference Time-Domain Method* (Artech House, Boston, 1996).
4. Y. Liu, Fourier analysis of numerical algorithms for the Maxwell equations, *J. Comput. Phys.* **124**, 396 (1996).
5. J. Fang, *Time Domain Finite Difference Computation for Maxwell's Equations*, Ph.D. dissertation (Department of Electrical Engineering, University of California, Berkeley, CA, 1989).
6. P. G. Petropoulos, Phase error control for FD-TD methods of second and fourth order accuracy, *IEEE Trans. Antennas Propagation* **42**, 859 (1994).
7. C. W. Manry, S. L. Broschat, and J. B. Schneider, Higher-order FDTD methods for large problems, *J. Appl. Comput. Electromag. Soc.* **10**, 17 (1995).
8. D. W. Zingg, J. Lomax, and H. Jurgens, High-accuracy finite-difference schemes for linear wave propagation, *SIAM J. Sci. Comput.* **17**, 328 (1996).
9. J. L. Young, D. Gaitonde, and J. J. S. Shang, Toward the construction of a fourth-order difference scheme for transient EM wave simulation: Staggered grid approach, *IEEE Trans. Antennas Propagation* **45**, 1573 (1997).
10. E. Turkel and A. Yefet, Fourth order accurate compact implicit method for the Maxwell quations, *Appl. Numer. Math.* **33**, 113 (2000).
11. E. Turkel and A. Yefet, A high order difference shceme for complex domains in a Cartesian grid, *Appl. Numer. Math.* **33**, 125 (2000).

12. J. S. Shang, High-order compact-difference schemes for time-dependent Maxwell equations, *J. Comput. Phys.* **153**, 312 (1999).
13. D. Gottlieb and B. Yang, Comparisons of staggered and non-Staggered schemes for Maxwell's equations, *12th Ann. Rev. Progress Appl. Comput. Electromag.* **2**, 1122 (1996).
14. M. K. Carpenter, D. Gottlieb, and S. Abarbanel, The stability of numerical boundary treatments for compact high-order finite-difference schemes, *J. Comput. Phys.* **108**, 272 (1993).
15. K. H. Dridi, J. S. Hesthaven, and A. Ditkowski, Staircase free finite-difference time-domain formulation for arbitrary material distributions in general geometries, submitted for publication.
16. A. Ditkowski, K. H. Dridi, and J. S. Hesthaven, Stable Cartesian grid methods for Maxwell's equations in complex geometries. I. Second order schemes, submitted for publication.
17. C. Zhang and R. J. LeVeque, The immersed interface method for acoustic wave equations with discontinuous coefficients, *Wave Motion* **25**, 237 (1997).
18. M. Ghrist, B. Fornberg, and T. A. Driscoll, Staggered time integrators for wave equations, *SIAM J. Numer. Anal.* **38**, 718 (2000).
19. J. J. Bowman, T. B. A. Senior, and P. L. E. Uslenghi, Eds., *Electromagnetic and Acoustic Scattering by Simple Shapes* (North-Holland, Amsterdam, 1969).
20. K. M. Mitzner, K. J. Kaplin, and J. F. Cashen, How scattering increases as an edge is blunted: The case of an electric field parallel to the edge, in *Recent Advances in Electromagnetic Theory*, edited by H. N. Kritikos and D. L. Jaggard (Springer-Verlag, New York, 1990), pp. 319–338.